

**Dissertation zur Erlangung des Doktorgrades  
der Fakultät für Chemie und Pharmazie  
der Ludwig-Maximilians-Universität München**



**Role of the CNGB1a Subunit of the Rod Cyclic Nucleotide-  
Gated Channel in Channel Gating and Pathogenesis of  
Retinitis Pigmentosa**

**Elvir Becirovic**

**aus Sarajevo**

**2010**

## **Erklärung**

Diese Dissertation wurde im Sinne von § 13 Abs. 3 bzw. 4 der Promotionsordnung vom 29. Januar 1998 von Prof. Dr. Martin Biel betreut.

## **Ehrenwörtliche Versicherung**

Hiermit versichere ich ehrenwörtlich, dass die vorgelegte Arbeit selbstständig und ohne unerlaubte Hilfe verfasst wurde. Es wurden keine anderen Hilfsmittel außer den angegebenen verwendet.

München, den .....

.....

(Elvir Becirovic)

Dissertation eingereicht am 16.4.10

1. Gutachter Prof. Dr. Martin Biel

2. Gutachter Prof. Dr. Christian Wahl

Mündliche Prüfung am 20.5.10

## Table of contents

1	Introduction .....	1
1.1	Anatomy of the retina.....	1
1.2	Anatomy of rods.....	2
1.3	Signalling transduction in rods .....	3
1.4	CNG channels .....	4
1.4.1	Topology and structural features of CNG channels .....	5
1.4.2	Gating of CNG channels .....	6
1.5	Role of CNGB1 in rod CNG channels .....	7
1.5.1	Characteristics of the <i>CNGB1</i> locus .....	7
1.5.2	Retinitis pigmentosa mutations in the <i>CNGB1</i> gene .....	7
1.6	Role of GARP in rods.....	8
1.7	Goals of this study .....	9
2	Materials and methods .....	10
2.1	Molecular biology.....	10
2.1.1	Plasmids .....	10
2.1.2	Polymerase chain reaction (PCR) .....	11
2.1.3	Purification of DNA fragments .....	11
2.1.4	Restriction analysis and preparation of samples for cloning .....	12
2.1.5	Ligation and dephosphorylation.....	12
2.1.6	Transformation.....	13
2.1.7	Inoculation of bacterial cells and isolation of plasmid DNA (alkaline lysis) .....	13
2.1.8	TOPO cloning.....	14
2.1.9	In-Fusion cloning.....	15
2.1.10	Introduction of mutations in DNA constructs.....	15
2.1.11	Reverse transcription (RT) .....	16
2.1.12	Cloning of CNG channels.....	16
2.2	Cell culture.....	16
2.2.1	Cultivation and transfection of mammalian cell lines.....	16
2.3	Protein biochemistry .....	17
2.3.1	Isolation and quantification of proteins .....	17
2.3.2	Membrane preparations .....	18
2.3.3	Western blotting .....	19
2.3.4	Co-immunoprecipitation .....	19
2.3.5	Biotinylation assay .....	20
2.4	Förster resonance energy transfer (FRET) .....	21

2.5	Electrophysiological recordings.....	21
2.6	Statistics .....	22
3	Results .....	23
3.1	Splicing analysis of the c.3444+1G>A mutation in <i>CNGB1</i> .....	23
3.1.1	<i>In silico</i> splicing analysis of c.3444+1G>A.....	23
3.1.2	Creation of wild type and mutant minigene constructs.....	24
3.1.3	Exon trapping experiments in HEK293T cells.....	25
3.1.4	<i>In vitro</i> expression of wild type and mutant rod CNG channels.....	26
3.2	Functional analysis of the G993V mutation in <i>CNGB1</i> .....	28
3.2.1	<i>In silico</i> analysis .....	28
3.2.2	Expression of CNGA1GV .....	30
3.2.3	Electrophysiological measurements of heteromeric CNGA1/CNGB1aGV channels.....	31
3.2.4	Coassembly and cell surface expression of CNGA1/CNGB1aGV heteromers.....	32
3.2.5	Identification of inhibitory domains in CNGB1a.....	34
3.2.6	Coexpression of GARP as soluble protein.....	37
3.2.7	Role of a functional CNBD of CNGB1 for CNG channel activation .....	39
3.2.8	Opening probability of channels containing or lacking the GARP domain.....	40
4	Discussion.....	42
4.1	Splicing analysis of the c.3444+1G>A mutation in <i>CNGB1</i> .....	42
4.2	Functional analysis of the G993V mutation in <i>CNGB1</i> .....	43
5	Summary.....	46
	Zusammenfassung .....	47
6	Literature.....	49
6.1	Cited publications .....	49
6.2	Own publications .....	52
	Accepted publications.....	52
	Publications under review or under revision.....	52
7	Appendix .....	53
7.1	Supplementary tables and figures.....	53
7.2	Abbreviations.....	59
7.3	Curriculum Vitae .....	61
	Lebenslauf.....	63
7.4	Acknowledgements/Danksagung.....	65

## 1 Introduction

### 1.1 Anatomy of the retina

The retina represents the light sensing part of the eye. It lines the back of the eye overlying the choroid layer. One characteristic of the vertebrate inverse retina is the fact that light has to pass the nerve cell layer until it reaches the photoreceptor cells. The latter consist of rods and cones and represent the light detecting part of the retina. The outer segments of photoreceptors are embedded in the light collecting pigment epithelium. In the adjacent outer nuclear layer (ONL) the cell bodies of rods and cones are located. Next to the ONL, in the outer plexiform layer (OPL) the synapses of rods and cones as well as of bipolar and horizontal cells are arranged. They are followed by the inner nuclear layer (INL) which is composed of cell bodies of bipolar, horizontal, and amacrine cells. Synaptic connections of bipolar cells to ganglion cells are situated in the inner plexiform layer (IPL). The cell bodies of the ganglion cells form the ganglion cell layer (GCL). The axons of the ganglion cells converge to the optic nerve and transmit the final output of the perceived light to the brain (Fig. 1).

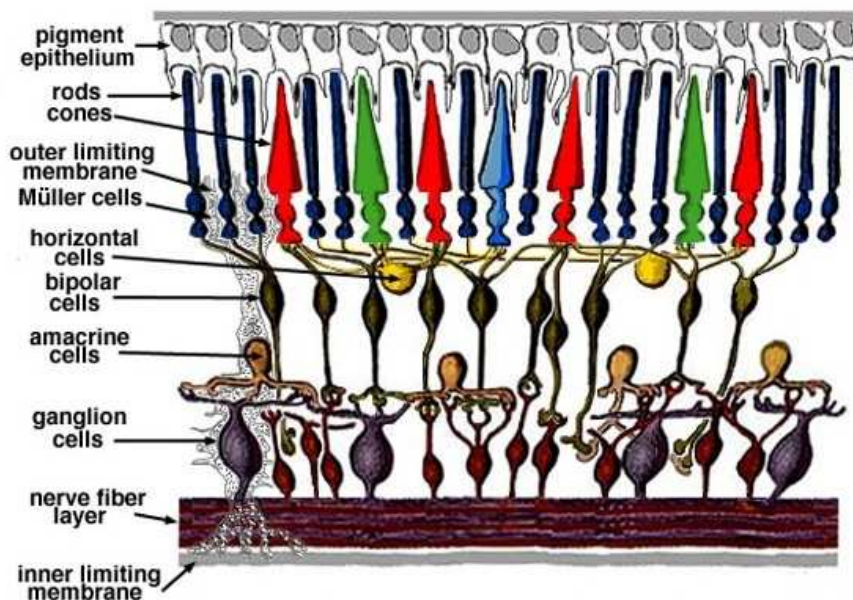


**Fig. 1 Schematic representation of the retinal structure.** Adapted from <http://webvision.med.utah.edu/sretina.html>.

## 1.2 Anatomy of rods

Rods and cones are the primary light sensitive cells of the retina. In contrast to cones which are specialized to the perception of daylight and colours (photopic system), rods are responsible for dim light vision (scotopic system). The schematic structure of a rod photoreceptor cell is shown in Fig. 2. A rod cell consists of an outer segment, an inner segment, the cell body and the synapse. The outer and inner segments are connected with a cilium that represents the bottleneck road for the transport of cargo from the cell body to the outer segments. Light detection and the downstream signalling transduction take place in the outer segments. Their interior space is filled with stacks of membranes called discs. The outer membrane encloses the outer segments and is the place of generation of the rod membrane potential.

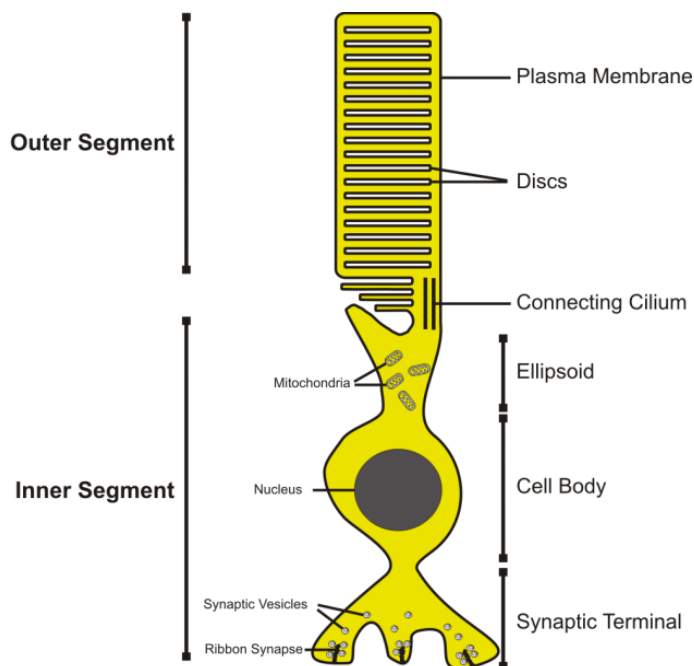


**Fig. 2 Schematic view of a rod photoreceptor.** Rods are composed of an outer segment that is connected to the inner segment via a connecting cilium. The outer segment is filled with discs which contain some members of the visual transduction cascade. The inner segment is composed of an ellipsoid (containing the mitochondria and the endoplasmic reticulum), the cell body and the synaptic terminal. The latter is filled with synaptic vesicles which converge on ribbon synapses and release the rod transmitter glutamate.

### 1.3 Signalling transduction in rods

Rods are able to detect even a single photon. This extremely high light sensitivity requires a massive signal amplification within the phototransduction cascade.

In dark, constitutively active guanylate cyclases (GCs) produce high cGMP levels. High cGMP levels in turn keep the cGMP sensitive cyclic nucleotide-gated (CNG) channel in its open state and give rise to the influx of  $\text{Na}^+$  and  $\text{Ca}^{2+}$ , respectively. This depolarises the rod cell up to -40 mV resulting in a “dark current”. Finally, this depolarisation triggers a sustained transmitter release at the synapse.

Photons are absorbed by retinal, a chromophore that is covalently attached to the G protein coupled receptor rhodopsin [1]. After absorption, retinal isomerizes from the 11-cis form to the all-trans form. This results in conformational changes of rhodopsin (bleaching). One of the intermediates of this bleaching process called metarhodopsin II ( $\text{Rh}^*$ ) activates the G protein transducin which stimulates the cGMP phosphodiesterase (PDE6) to hydrolyse cGMP to GMP. The decrease in cGMP concentration in turn leads to the closure of the CNG channel. As a consequence, the outer membrane hyperpolarises to -70 mV [2] and gives rise to the switch-off of transmitter release to bipolar cells. Thus, the light signal information finally sent to the brain is generated by the termination (and not by the generation) of transmitter release.

In order to regenerate the dark current, the rod cell has to restore the cGMP concentration to the dark level. This process is regulated by the  $\text{Ca}^{2+}$  concentration and by the action of guanylate cyclases (GC-E/F). The latter are controlled by guanylate cyclase activating proteins (GCAPs). In their inactive form, GCAPs bind  $\text{Ca}^{2+}$  molecules. During light response, the CNG channel is closed and the  $\text{Ca}^{2+}$  levels are low [3]. The decrease in  $\text{Ca}^{2+}$  levels converts GCAP to the active form which then stimulates GCs to produce cGMP. High cGMP levels finally lead to opening of CNG channels and to the restoration of the dark current (Fig. 3 A).

Several other mechanisms ensure the inactivation of the signalling cascade and influence the photoresponse kinetics. One of them includes the inactivation of  $\text{Rh}^*$  by phosphorylation. This step is catalyzed by the rhodopsin kinase [4]. Another protein called arrestin binds to phosphorylated rhodopsin and prevents it from activation of transducin [5]. Subsequently, all-trans retinal is replaced by 11-cis retinal and rhodopsin becomes dephosphorylated. This finally gives rise to the recurrence of rhodopsin to its inactive state (Fig. 3 B).

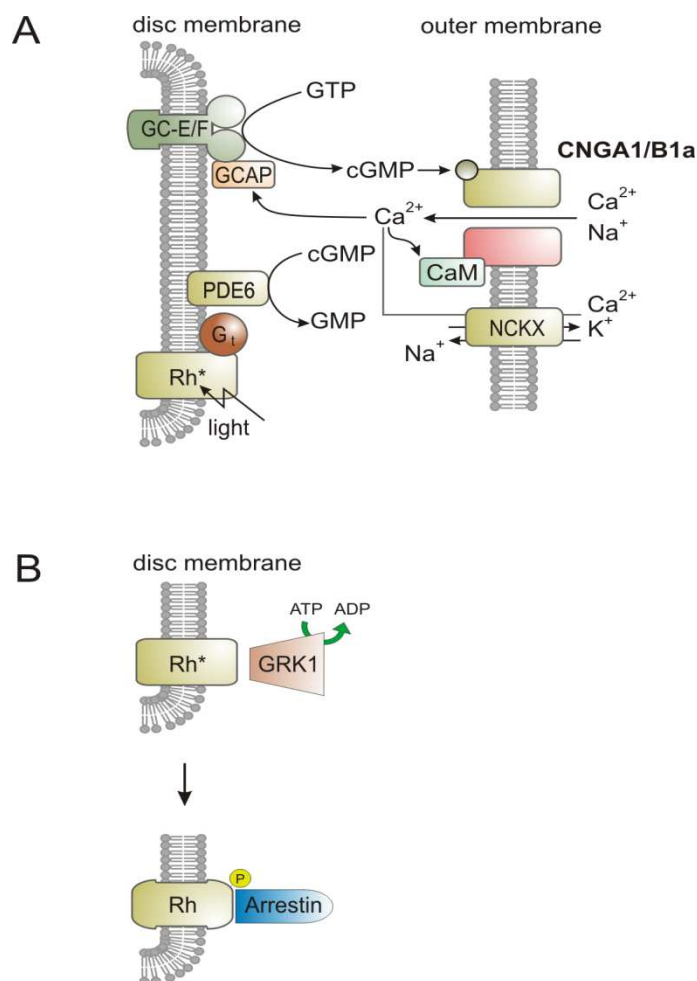


**Fig. 3 Signalling transduction in rods.** A) Molecular mechanisms occurring in the rod outer segments upon light induced rhodopsin activation. B) Phosphorylation of Rh\* by rhodopsin kinase (GRK1) gives rise to binding of arrestin which prevents rhodopsin from sustained activation of transducin. For details, see text. NCKX, Na<sup>+</sup>/Ca<sup>2+</sup>/K<sup>+</sup> exchanger; G<sub>t</sub>, transducin; CaM, calmodulin.

### 1.4 CNG channels

Cyclic nucleotide-gated channels are nonselective cation channels that translate changes in the concentration of cAMP or cGMP into an electrical response and/or an intracellular Ca<sup>2+</sup>-signal. Although CNG channels are expressed in different tissues, their function in vertebrates has been well characterised only in photoreceptors and olfactory sensory neurons so far. Native CNG channels are heterotetramers consisting of A and B subunits which together form the central ion conducting pore. The subunit expression and composition of CNG channels is tissue dependent. As depicted in Fig. 4, CNG channels from rods are composed of three CNGA1 and one CNGB1a subunit [6-8]. In contrast, the cone CNG channel comprises two CNGA3 and two CNGB3 subunits [9], and in the olfactory epithelium, two CNGA2, one CNGA4 and one CNGB1b form the native CNG channel [10].

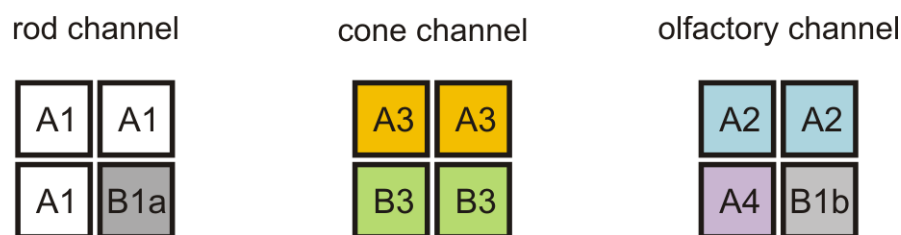


**Fig. 4 Subunit composition of CNG channels.**

### 1.4.1 Topology and structural features of CNG channels

CNG channels belong to the superfamily of voltage-gated ion channels. The members of this channel group consist of an intracellular N-terminus, six transmembrane domains (S1-S6) and an intracellular C-terminus. Transmembrane segments of CNG channels are connected to each other by short loops. The last loop located between S5 and S6 forms the pore region. The C-terminal domain is subdivided into three functional domains: C-linker, cyclic nucleotide-binding domain (CNBD) and the distal C-terminus [11, 12].

CNG channels are structurally and evolutionary related to hyperpolarisation activated cyclic nucleotide-gated (HCN) channels. Recently, the crystal structure of the C-terminus of HCN channels consisting of the C-linker and the CNBD was determined (Fig. 5, [13]). The comparison of the CNBD of HCN channels to that of other cyclic nucleotide-binding proteins like the gene activator protein (CAP, [14]) and cAMP dependent protein kinase (PKG1, [15]) reveals that these proteins share very similar folding properties. The C-linker comprises six  $\alpha$ -helices (A'-F') followed by an  $\alpha$ -helix of the CNBD and a  $\beta$ -roll consisting of eight  $\beta$ -strands (1-8). Another short  $\alpha$ -helix (called P-helix) is located between  $\beta$ -strands 6 and 7. The last  $\beta$ -strand is followed by two additional  $\alpha$ -helices (B- and C-helix, respectively).

C-linker and CNBD have been extensively analysed and have been shown to be involved in channel gating processes. In contrast, the function of the distal C-terminus has been less well-characterised so far. However, this domain has been shown to play an important role in channel targeting to the outer membrane of the rod outer segments [16, 17].

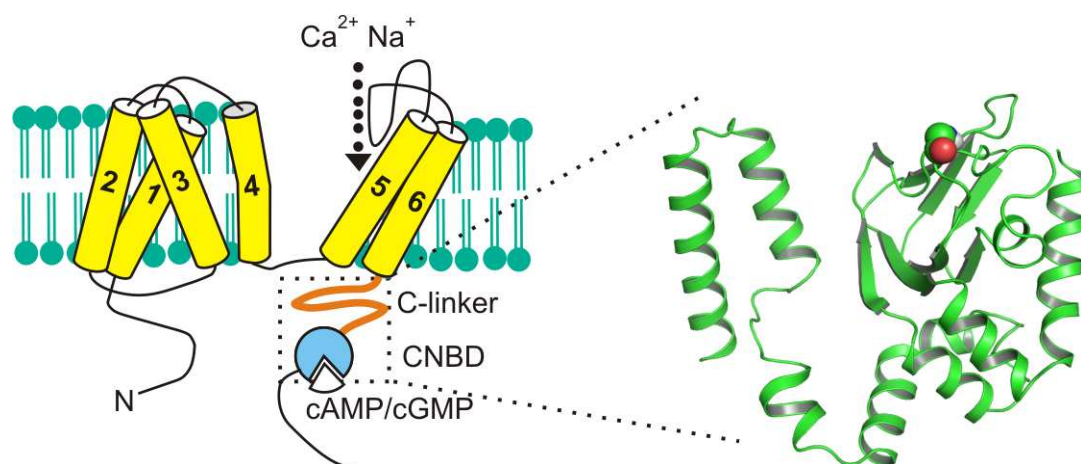


**Fig. 5 Topology of CNG channels.** Left: representative topology of a CNG subunit consisting of the intracellular N- and C-terminus and six transmembrane domains (1-6). Right: 3D model of the C-terminus of CNGB1a based on the molecular dynamics (MD) simulation performed by the group of Prof. Dr. Klaus T. Wanner, Department of Chemistry, Ludwig Maximilians Universität München. MD simulation was based on the recently identified crystal structure of the C-terminus of HCN2 [13]. For details, see text.

#### 1.4.2 Gating of CNG channels

As mentioned above, CNG channels principally can be activated by both cGMP and cAMP. However, the ligand affinity, efficacy, open probability, ion permeability or adaptation strongly depend on the respective subunit compositions. For example, olfactory CNG channels show a similar sensitivity to cAMP and cGMP whereas in rod photoreceptors, the sensitivity of the CNG channel to cGMP is much higher compared to cAMP [18, 19]. Electrophysiological measurements indicate that gating of CNG channels occurs in a cooperative manner. Additionally, it has been shown that the binding of only two ligands is sufficient to fully activate the channel. Binding of the remaining two ligands is proposed to have only stabilising effects on the open conformation of the channel [20]. Moreover, a preferential order of ligand binding to the single subunits also seems to exist, as demonstrated recently for olfactory CNG channels [21]. Ligand binding to CNGB1b subunit was proposed to occur after the binding of the first two ligands to CNGA4 and CNGA2, respectively. Thus, it was concluded that CNGB1b is not involved in the initial opening of the channel but rather in stabilising its open state.

## 1.5 Role of CNGB1 in rod CNG channels

### 1.5.1 Characteristics of the *CNGB1* locus

The *CNGB1* locus is a complex gene giving rise to the transcription of at least four different variants due to alternative splicing. In rod photoreceptors, three transcripts deriving from the *CNGB1* gene and encoding CNGB1a, GARP1 and GARP2 could be identified [22-24]. In olfactory sensory neurons, only CNGB1b is expressed [25]. This splice isoform lacks the most part of the long amino terminus which is present in CNGB1a.

In contrast to CNGA1, CNGB1a subunit is not able to form functional channels when expressed alone in heterologous expression systems. However, when coexpressed with CNGA1 the CNGB1a subunit confers several characteristic properties to the heteromeric channel [24]. For example, heteromeric CNGA1/CNGB1a channels show an increased sensitivity to cAMP and are efficiently blocked by L-cis-diltiazem. Furthermore, CNGA1/CNGB1a heteromers show a typical single channel flickering behaviour, an increased inhibition by calmodulin (CaM), and a decreased block by extracellular  $Ca^{2+}$  [11, 12, 26, 27].

The involvement of CNGB1 in the transport of heteromeric channels to their final destination represents another important function of this subunit. In the *CNGB1* KO model, the transport of CNGA2 and CNGA4 to the olfactory cilia as well as the transport of CNGA1 to the outer segments is strongly impaired [28, 29]. Recently, some aspects of the molecular mechanisms regarding the transport of CNG channels to olfactory cilia and outer segments of rod photoreceptors could be clarified. It has been shown that the distal C-terminus of CNGB1a plays a crucial role in this process [17, 30].

### 1.5.2 Retinitis pigmentosa mutations in the *CNGB1* gene

Retinitis pigmentosa (RP) is a severe hereditary eye disorder characterised by progressive degeneration of photoreceptors and subsequent loss of vision. Degeneration of rod photoreceptors is accompanied by loss of dim light vision and by an impairment of contrast perception. In later stages of the disease, as a secondary effect, cone photoreceptors often also undergo degeneration leading to total blindness. Depending on the affected gene and/or the kind of the corresponding mutation, the inheritance of RP may be dominant or recessive. In human patients, numerous mutations in different genes have been shown to be causative for RP. Many of the RP causing genes encode for members of the signalling transduction cascade. Among the rod CNG channel subunits, the vast majority of RP associated mutations were identified in the CNGA1 subunit. There are also two reports linking mutations

in the *CNGB1* locus to recessive form of RP [31, 32]. One of these mutations (c.3444+1G>A) represents a splice site mutation positioned on the donor site of Exon 32, the other one (c.2978G>T; p.G993V) represents a point mutation located in the CNBD of *CNGB1*. However, so far no functional analysis of these two mutations was performed in order to verify their pathogenicity or to decipher the molecular mechanism leading to the RP phenotype.

### 1.6 Role of GARP in rods

The exact molecular functions of the glutamic acid rich proteins, GARP1 and GARP2 (herein referred to as GARPs) have not been well characterised so far. GARPs are soluble proteins and represent alternatively spliced isoforms of the *CNGB1* gene (see chapter 1.5.1). The protein sequence of GARPs is almost completely identical to the respective region of the N-terminus of *CNGB1a*. In contrast to GARP1, GARP2 lacks the negatively charged glutamic acid rich region and is expressed at high levels in rod outer segments [23, 24, 33].

Disc rims are regions of the rod disc membranes adjacent to the rod plasma membrane. It has been reported that GARP2 interacts with different disc rim associated proteins, like peripherin-1 or PDE6 [33-35]. Some of the proposed functions of GARPs arising from these studies are the fine-tuning of the cGMP signalling and scaffolding functions, like the maintenance of the disc rim integrity and tethering of CNG channels to disc rims. Most probably because of their high content of charged glutamic acids, GARPs were also shown to have features of natively unfolded proteins [33].

In contrast to *CNGB1* KO mice which do not lack GARPs [28], *CNGB1* KO mice deficient for both, *CNGB1a* and GARPs show an impaired structure of outer segments and a spoiled discs morphogenesis [36]. However, there are no specific GARP1 or GARP2 KO mice available so far.

## 1.7 Goals of this study

This study was set out to address two important questions:

- 1) How do specific mutations in the *CNGB1* gene result in RP?
- 2) What is the role of CNGB1a in gating of rod CNG channels?

The main focus of this study was to answer these questions by functional analysis of the two RP causing mutations in the *CNGB1* gene.

As described in chapter 1.5.2, the first mutation (c.3444+1G>A) represents a splice site mutation positioned on the donor site of Exon 32. This mutation could impact CNGB1a on mRNA and on protein level and was therefore tested for splicing and expression in HEK293T cells.

The second mutation (c.2978G>T; p.G993V) is a point mutation located in the CNBD of CNGB1a. Since this domain is crucial for proper gating of the CNG channel, the p.G993V mutation harbours the potential to impair the gating of these channels. The effects of this mutation on channel gating were analysed by different computational, electrophysiological, and protein biochemical experiments.

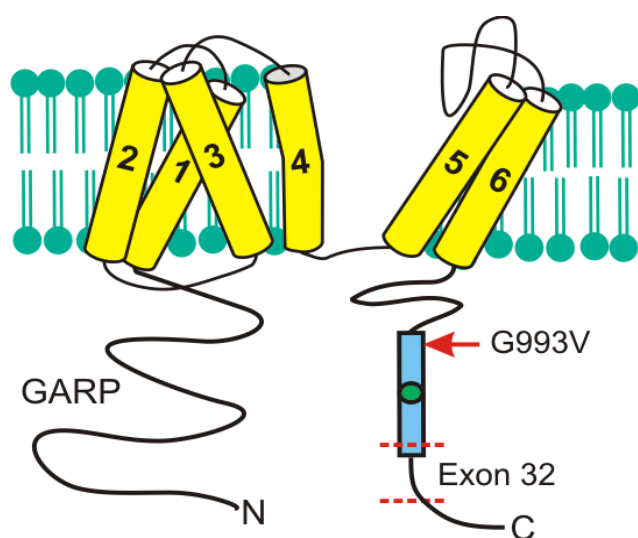


**Fig. 6 RP mutations in CNGB1a.** Blue box marks the CNBD, green circle shows the position of the cGMP binding pocket, and the red arrow the position of the G993V mutation. Since the c.3444+1G>A mutation is a splice site mutation located on the donor site of exon 32, its position cannot be marked on protein level. Instead, the region in CNGB1a encoded by exon 32 (flanked by two red dashed lines) is shown. GARP, glutamic acid rich protein domain.

## 2 Materials and methods

### 2.1 Molecular biology

#### 2.1.1 Plasmids

##### pcDNA3.1 vector

pcDNA3.1 (Invitrogen) represents a commonly used mammalian expression vector. It consists of following elements:

- Cytomegalovirus (CMV) promoter, capable of driving heterologous gene expression in mammalian cell lines.
- Simian virus (SV40) origin of replication (ori), allowing for replication in mammalian cells.
- Colicinogenic factor E1 (ColE1) ori, responsible for replication in prokaryotes.
- Filamentous phage (f1) ori which allows recovery of single stranded plasmids in prokaryotes.
- Multiple cloning site (MCS) for introduction of genes or gene fragments of interest.
- Polyadenylation signal (pA) of the bovine growth hormone (BGH).
- Neomycin resistance (Neo<sup>R</sup>) under the control of SV40 promoter for selection of stable mammalian cell lines.
- Ampicillin resistance (Amp<sup>R</sup>) for selection of recombinant bacterial cells.

##### pCRII<sup>®</sup>-TOPO<sup>®</sup> vector

This vector was used for subcloning of PCR products (see chapter 2.1.8). It contains a lacZ promoter followed by the MCS and lacZ reporter gene. Thus, insertion of constructs into the MCS disrupts the expression of  $\beta$ -galactosidase and can be used for selection of recombinant bacterial clones on X-gal containing plates. Additionally, this vector contains a f1 ori and pUC ori for plasmid replication in prokaryotes. For selection of recombinant bacteria, kanamycin and ampicillin resistance (Amp<sup>R</sup>) are included in this vector.

##### pIRESeGFP vector

pIRESeGFP vector allows the gene of interest and enhanced green fluorescent protein (eGFP) to be expressed simultaneously but separately from a bicistronic mRNA. This is assured by the presence of an internal ribosome entry site (IRES) of encephalomyocarditis virus (EMCV) located between the MCS and coding region of GFP. Additionally, this vector contains following elements:

CMV promoter, SV40 pA, SV40 promotor, SV40 ori, f1 ori, Kan<sup>R</sup>, Neo<sup>R</sup>, pUC ori and the herpes simplex virus thymidine kinase (HSV-TK) pA.

### 2.1.2 Polymerase chain reaction (PCR)

The conditions of each PCR reaction were adjusted to the respective application. Table 1 shows an overview about the standard PCR conditions of different polymerases used in this study:

**Table 1 Standard PCR conditions for different polymerases.**

Polymerase	Taq	Pfu (Stratagene)	Herculase (Stratagene)	Phusion (Finnzymes)
Initial denaturation	95°C 1 min	95°C 1 min	95°C 1 min	98°C 30 sec
Denaturation	95°C 30 sec	95°C 45 sec	95°C 20 sec	98°C 10 sec
Annealing	X °C 30 sec	X °C 45 sec	X °C 20 sec	X °C 30 sec
Elongation	72°C 30 sec/kb	72°C 1 min/kb	72°C 30 sec/kb	72°C 30 sec/kb
Final elongation	72°C 5 min	72°C 5 min	72°C 5 min	72°C 5 min
Storage	10°C ∞	10°C ∞	10°C ∞	10°C ∞

} 35 x

The pipetting scheme of the PCR was adapted from the manual of the respective manufacturer.

### 2.1.3 Purification of DNA fragments

After PCR amplification, the PCR products may be purified for further applications. The purification was performed using the PureLink<sup>TM</sup> Quick Gel Extraction Kit (Invitrogen) according to manufacturer's protocol. All solutions needed for this procedure were provided with the kit. Briefly, fivefold amount of solubilization buffer was added to the PCR product and the solution was loaded on the column. The latter was placed in 2 mL Eppendorf tubes and was centrifuged at max. speed for 45 sec at room temperature. The flow through was discarded and 700 µL wash buffer was added to the column following by an additional centrifugation at identical conditions. After discarding the flow through, the column was spun at max. speed for 2 min at room temperature in order to remove all ethanol present in the wash buffer. Now, 30 µL ddH<sub>2</sub>O or elution buffer was added on the center of the column which was allowed to incubate 10 min at room temperature. Finally, the DNA was eluted into a fresh 1.5 mL Eppendorf tube by centrifugation at max. speed for 45 sec at room

temperature. To check for proper purification, 5  $\mu\text{L}$  of the purified DNA were loaded on agarose gel.

#### 2.1.4 Restriction analysis and preparation of samples for cloning

Restriction enzymes were purchased from New England BioLabs (NEB) or from Fermentas. Restriction analysis conditions were performed following the manufacturer's instructions. For cloning applications, the amount of DNA in the restriction reaction was 3-5  $\mu\text{g}$ . After the incubation time, the cut DNA was loaded on the appropriate agarose gel and was allowed to run until sharp bands could be cut off from the gel. Then, the cut piece of gel was weighed and the threefold volume of gel solubilization buffer (PureLink™ Quick Gel Extraction Kit, see chapter 2.1.3) was added (i. e. if the gel piece weighed 200 mg, the amount of gel solubilization buffer was 600  $\mu\text{L}$ ). Now, the sample was incubated at 55°C for 5-10 min or until the gel was completely solved. This solution was loaded on the columns from the Quick Gel Extraction Kit and the the same procedure as described in chapter 2.1.3 was performed.

#### 2.1.5 Ligation and dephosphorylation

Ligation reaction was performed using following pipetting scheme:

x  $\mu\text{L}$  vector DNA  
y  $\mu\text{L}$  insert DNA  
2  $\mu\text{L}$  T4 ligase buffer (NEB)  
1  $\mu\text{L}$  T4 ligase (NEB)  
20  $\mu\text{L}$  total volume

This reaction was incubated for 30 min - 2 h at room temperature. The vector-to-insert ratio was variable and was determined empirically for each ligation considering the amount of the respective DNA observed on the check agarose gel after the DNA purification. After the ligation vector DNA was dephosphorylated by following protocol:

3  $\mu\text{L}$  of the Fast AP buffer and 2  $\mu\text{L}$  of Fast AP (Fermentas) were added to the ligation reaction which was then incubated at 37°C for 10 min. Subsequently, the enzyme was heat inactivated by incubating the reaction at 65°C for 15 min.

### 2.1.6 Transformation

For transformation different chemically competent *E.coli* strains were used depending on the application. First, 100  $\mu\text{L}$  aliquots of competent cells (stored at  $-80^{\circ}\text{C}$ ) were thawed on ice. Then, 1-3  $\mu\text{L}$  DNA (i. e. ligation reaction) were added to the cell suspension which was gently swirled and was allowed to incubate on ice for 5 min. Now, a heat pulse was applied by incubating the cells for 30 sec at  $42^{\circ}\text{C}$  in a water bath. Immediately after this, the cell suspension was placed on ice for 2 min. If the resistance for selection of the plasmid DNA was ampicillin, the cells were directly plated on the appropriate agar plates. In cases of chloramphenicol or kanamycin resistance, 900  $\mu\text{L}$  prewarmed LB(+) medium was added to the cells. The latter were incubated for 1 h at  $37^{\circ}\text{C}$  with shaking followed by a centrifugation at 3500 rpm for 5 min at room temperature. Approx. 800  $\mu\text{L}$  of the supernatant was removed and the cells were resuspended in the remaining part of the LB(+) medium. Finally, the cells were plated on the respective agar plates and incubated over night at  $37^{\circ}\text{C}$ .

#### LB(+) medium

Pepton            10 g  
Yeast extract    5 g  
NaCl              5 g  
Glucose          1 g  
ddH<sub>2</sub>O          ad 1 L  
adjust pH to 7.2 - 7.5  
autoclave

#### LB(+) Agar

Agar 15 g  
LB(+) medium ad 1 L  
autoclave  
for preparing resistant agar plates, cool the LB(+) agar medium to  $55^{\circ}\text{C}$  and add the appropriate resistance in concentrations described in chapter 0.

### 2.1.7 Inoculation of bacterial cells and isolation of plasmid DNA (alkaline lysis)

Bacterial clones were picked from the plate and were transferred to 10 mL polypropylene tubes containing the LB(+) medium with the appropriate resistance (ampicillin: 100  $\mu\text{g}/\text{mL}$ , kanamycin: 30  $\mu\text{g}/\text{mL}$ , chloramphenicol: 30  $\mu\text{g}/\text{mL}$ ). Then, the suspension was incubated over night at  $37^{\circ}\text{C}$  with shaking (225 rpm). On the next day, the cells were spun at 1000 x g for 10 min at room temperature or at  $4^{\circ}\text{C}$  and were resuspended in 250  $\mu\text{L}$  resuspension buffer. This solution was transferred into 2 mL Eppendorf tubes. After adding 250  $\mu\text{L}$  lysis buffer the cell suspension was inverted several times and was allowed to incubate for max. 5 min at room temperature. Now, 250  $\mu\text{L}$  neutralization solution was added to the mix, was inverted, and was incubated for 5 min at room temperature. Next, the suspension was centrifuged at rpm max. for 15 min at  $4^{\circ}\text{C}$  or at room temperature. The supernatant

containing the plasmid DNA was transferred into fresh 1.5 mL Eppendorf tubes. To precipitate DNA, 520  $\mu\text{L}$  100 % isopropanol was added to the mix. After vortexing, the mix was spun at rpm max. for 15 min at 4°C. Subsequently, the pellet was washed with 70 % ethanol and the solution was centrifuged at rpm max. for 5 min at 4°C. Then, the supernatant was discarded and the pellet was dried in a vacuum centrifuge at room temperature for 5 min. Now, the pellet was suspended in 30  $\mu\text{L}$  of ddH<sub>2</sub>O and 1  $\mu\text{L}$  of this plasmid DNA solution was used for control restriction analysis. If the expected results were obtained from this restriction analysis, the corresponding plasmid DNA was sent for sequencing without further purification.

To yield plasmid DNA in larger amounts and in higher purity, PureYield™ Plasmid Midiprep System (Promega) was used. For that purpose, colonies were inoculated in 100-200 mL LB(+) medium and similar procedure as described above was performed following the manufacturer's instructions.

### 2.1.8 TOPO cloning

TOPO cloning (TOPO TA Cloning® Kit Dual Promotor, Invitrogen) represents a rapid and convenient cloning method for PCR products. Topoisomerase I from *Vaccinia* virus [37] attached to the pCRII®-TOPO® vector allows for covalent bonding of PCR products to this vector. However, this reaction only takes place if the respective PCR product possesses a deoxyadenosine (A) on its 3' end. In contrast to most polymerases with proof reading activity (i.e. Pfu-polymerase), conventional Taq polymerase has terminal transferase activity that adds a single "A" to the 3' ends of the PCR products.

First, PCR products which were amplified using a polymerase without terminal transferase activity were purified by standard procedures as described in chapters 2.1.3 and 2.1.4. Then, following components were added to 8  $\mu\text{L}$  of the purified PCR product:

0.5  $\mu\text{L}$  dNTP (10 mM each)

1  $\mu\text{L}$  Taq buffer (containing 2.5 mM MgCl<sub>2</sub>)

0.5  $\mu\text{L}$  Taq-Polymerase

This reaction was incubated for 30 min at 72°C and was placed on ice. TOPO cloning reaction was performed using following pipetting scheme:

4.5  $\mu\text{L}$  of the Taq polymerase reaction product

1  $\mu\text{L}$  salt solution (provided with the kit)

0.5  $\mu\text{L}$  TOPO vector (provided with the kit)

The mix was incubated for 20 min at room temperature and 2-3  $\mu\text{L}$  were used for transformation of chemically competent bacterial cells as described in chapter 2.1.6.

### 2.1.9 In-Fusion cloning

For some cloning applications, as an alternative to mutagenesis PCR and/or overlap-PCR, In-Fusion™ Advantage PCR Cloning Kit (Clontech) was used. PCR products sharing a 15 bp homology with the sequence at the ends of the linearized vector can be covalently attached to the vector giving rise to circular plasmid DNA. The In-Fusion enzyme provided with the kit catalyzes this covalent bonding.

The In-Fusion reaction was set up as follows:

≈ 100 ng purified PCR product

≈ 200 ng purified vector

2 μL 5 x In-Fusion reaction buffer

1 μL In-Fusion enzyme

Ad 10 μL ddH<sub>2</sub>O

If larger volumes of vector or insert were used, the volume of buffer, of the enzyme and the total volume were doubled. The In-Fusion mix was now incubated at 37°C for 15 min following by an incubation at 50°C for 15 min. Then, the reaction was placed on ice and diluted in TE buffer (pH 8.0) up to a volume of 50 μL. Finally, 3-5 μL of this solution were used for a standard transformation protocol.

### TE Buffer

10 mM Tris-HCl pH 8.0

3 mM EDTA

### 2.1.10 Introduction of mutations in DNA constructs

In most cases, mutations were introduced by means of site directed mutagenesis. Site directed mutagenesis PCR was performed using the QuickChange XL Site-Directed Mutagenesis Kit (Stratagene) according to manufacturer's instructions or by overlap-PCR. The latter requires a two-step PCR reaction. Thereby, the choice of appropriate overlap primers allows for deletion or insertion of desired DNA sequences. In the first PCR reaction, two separate PCR products were amplified which share a sequence homology ("overlap") at their 3' ends. After the purification of the PCR products by gel extraction, they were used as DNA template for the second PCR reaction. Routinely, in this study overlap PCR was performed using the Pfu polymerase.

### 2.1.11 Reverse transcription (RT)

Reverse transcription was performed using the ThermoScript™ RT-PCR System Kit (Invitrogen) following the instructions of the manufacturer. During the cDNA synthesis, random hexamers as well as oligo(dT) primer were added to the reaction. After the cDNA synthesis, herculase (Stratagene) was used for the subsequent PCR.

### 2.1.12 Cloning of CNG channels

Cloning of the rat CNGB1a/CNGB1b and CNGA2/CNGA4 subunits was described previously [25, 38, 39]. Bovine CNGA1 was a gift of Dr. U. Benjamin Kaupp (Caesar Bonn). As far as not otherwise mentioned, all experiments from the electrophysiological and biochemical recordings described in chapter 3.2 were obtained using rat CNGB1 and bovine CNGA1 channels. Human CNG channels were PCR amplified from retinal cDNA, were subcloned into the pcDNA3.1 and/or pIRESeGFP vector and sequenced.

## 2.2 Cell culture

### 2.2.1 Cultivation and transfection of mammalian cell lines

For most *in vitro* transfections in this study, HEK293T cells were used. They were cultivated in DMEM + GlutaMAX™-I medium (+ 4,5 g/L glucose, - pyruvate + 10 % FBS + 1 % penicillin/streptomycin) at 37°C with 10 % CO<sub>2</sub>. COS7 cells were cultivated under same conditions in DMEM + GlutaMAX™-I medium (+ 4,5 g/L glucose, + pyruvate + 10 % FBS + 1 % penicillin/streptomycin).

Transient transfections of HEK293T cells or COS7 cells were performed using the calcium phosphate technique [40] or with FuGENE® (Promega). The calcium phosphate based transfection was performed by adding following solutions to a 15 mL Falcon tube:

10     μg DNA,  
50     μL 2,5 M CaCl<sub>2</sub>  
ad 500 μL ddH<sub>2</sub>O

While vortexing this mix, 2 x BBS solution was added drop wise. Then, the mix was incubated for max. 5 min at room temperature. This mixture was added drop wise to the 40-70 % confluent cells which subsequently are incubated at 37°C with 3-5 % CO<sub>2</sub>. 8-16 h after the transfection, medium was replaced and the cells were incubated at 37°C with 10 % CO<sub>2</sub> until harvesting. The amounts of different components described above

correspond to  $\varnothing$  10 cm plates. For  $\varnothing$  15 cm plates, the volume of all solutions was doubled and the amount of DNA was increased to 25-30  $\mu\text{g}$ .

Transfection with FuGENE<sup>®</sup> (Roche) was performed for subsequent immunocytochemical and electrophysiological applications. For 16-well plates 30 ng DNA was used per well, for  $\varnothing$  3.5 cm plates 3  $\mu\text{g}$  DNA was used. First, fresh GlutaMAX<sup>™</sup>-I medium (without FBS and without penicillin/streptomycin) was added to cryo tubes followed by the addition of DNA. Thereby, tenfold volume of medium related to the total volume on DNA was added (i. e. 1  $\mu\text{L}$  DNA corresponds to 10  $\mu\text{L}$  medium). After the 5 min incubation, FuGENE was added directly to the reaction which was mixed subsequently by pipetting up and down. In this case, threefold volume of FuGENE in  $\mu\text{L}$  was used related to the amount of DNA in  $\mu\text{g}$  (i. e. 1  $\mu\text{g}$  DNA corresponds to 3  $\mu\text{L}$  FuGENE). This reaction was allowed to incubate for 30 min at room temperature and was then added directly to the medium of the cells. The latter were incubated at 37°C with 10 % CO<sub>2</sub> until proceeding with the respective application.

## **2 x BBS Solution**

10,65 g BES

16,35 g NaCl

0,21 g Na<sub>2</sub>HPO<sub>4</sub> · 2H<sub>2</sub>O

ad 950 mL H<sub>2</sub>O

adjust to pH 6,95 with NaOH

ad 1L ddH<sub>2</sub>O

steril filtrate

## **2.3 Protein biochemistry**

### **2.3.1 Isolation and quantification of proteins**

Proteins were isolated from cultured mammalian cells by the following protocol:

48 h after transfection, medium was removed and the cells were harvested in a 1.5 mL Eppendorf tube. Then, the suspension was centrifuged at 4°C for 5 min at 1000 x g. Hereafter, the pellet was resuspended in lysis buffer and was rotated at 4°C for 30 min. Subsequently, the cells were spun at 4°C for 10 min at rpm max. and the supernatant was transferred into a fresh 1.5 mL Eppendorf tube.

For protein isolation from mouse tissue, the latter was suspended in lysis buffer containing the proteinase inhibitor cocktail mix (Roche) and the tissue disruption was performed using the Potter S homogenizer (B. Braun Biotech International). Then, the suspension was

centrifuged at 4°C at rpm max. and the supernatant was transferred into fresh 1.5 mL Eppendorf tubes.

To determine the concentration of isolated proteins, Bradford assay was performed [41]. Thereby, 5 µL of the protein solution (5 µL lysis buffer were used as blank control) were transferred into 1 mL plastic cuvettes followed by an addition of 95 µL 0.15 M NaCl solution. Then, 1 mL coomassie blue solution was added and was allowed to incubate for 2 min at room temperature. Immediately after the incubation time, protein concentration was measured using the Bradford assay program on the BioPhotometer (Eppendorf).

### **1 x Lysis Buffer**

2.5 mL Triton X-100

15 mL 5 M NaCl

400 µL 2.5 M CaCl<sub>2</sub>

### **Coomassie Blue Solution**

50 mg coomassie brilliant blue G250

25 mL 95 % ethanol

50 mL 85 % phosphoric acid (H<sub>3</sub>PO<sub>4</sub>)

ad 500 mL ddH<sub>2</sub>O

### **2.3.2 Membrane preparations**

For enrichment of membrane proteins, preparations of cell membranes were performed. For this purpose, 1-2 mL of the 1 x membrane preparation buffer containing the proteinase inhibitor cocktail mix was added to the harvested HEK293T cells or mouse tissue and the breakup of cell or of the tissue was performed using the Potter S homogenizer. Then, the suspension was centrifuged at 4°C for 10 min at 500 0 x g. The supernatant was transferred into 6 mL ultracentrifuge tubes and 1 x membrane preparation buffer was added to a final volume of 4 mL. Ultracentrifugation was performed at 4°C for 45 min at 30000 rpm (Beckman 45 Ti rotor). Pellet was suspended in 50-100 µL 1 x membrane preparation buffer and 5 µL were used for determination of the protein concentration as described in chapter 2.3.1.

### **3 x Membrane Preparation Buffer:**

3,15 g MOPS

77 g Sucrose

6 mL 0.5 M EDTA (pH 7.4)

ad 250 mL ddH<sub>2</sub>O

### 2.3.3 Western blotting

Western blotting was performed by standard procedures. After the protein transfer to the PVDF membrane, the latter was shortly equilibrated with methanol and was blocked in 5 % milk powder for 1 h at room temperature with shaking. Then, the incubation of the membrane with the appropriate primary antibody was performed. The optimal incubation time and the optimal antibody concentration were determined empirically. Hereafter, the membrane was washed three times in TBST for 5 min followed by an 1-2 h incubation with the secondary antibody at room temperature with rotation. Now, the membrane was washed 3-4 times with TBST for 5 min and once in ddH<sub>2</sub>O. After the incubation with the luminol reagent according to manufacturer's protocol (Millipore or Santa Cruz), the membrane was put into a film cassette and was exposed to a x-ray film (Fuji). The optimal exposure time was determined empirically.

#### 10 x TBS

12.1 g Tris  
80.2 g NaCl  
ad 1 L ddH<sub>2</sub>O

#### 1 x TBST

100 mL TBS  
0.1 % Tween  
protect from light

### 2.3.4 Co-immunoprecipitation

To analyse protein-protein interactions, co-immunoprecipitation experiments using protein G dynabeads (Invitrogen) were performed. First, approx. 5 µg antibody and PBS were added to 30 µL dynabeads up to a final volume of 500 µL. This solution was rotated for 30 min at 4°C and subsequently, the supernatant was removed on the magnet followed by a wash step with 200 µL PBS. Then, 1 mg of the protein lysate was added to the beads and the reaction was filled up with PBS to a final volume of 500 µL. Now, the suspension was rotated for 30 min at 4°C followed by three washing steps with PBS. After the last wash, the suspension was transferred into fresh 1.5 mL Eppendorf tubes and the supernatant was removed completely. Beads were resuspended in 6 x Lämmli buffer (with or without DTT, depending on the application) and were incubated at 70°C for 15 min. Finally, the supernatant was loaded on the appropriate SDS PAGE gel.

In some cases, the antibody and IgG's of protein G were crosslinked to the beads by means of irreversible, non-cleavable crosslinker BS3 (Thermo Scientific). For this purpose, after the coupling of the antibody to the beads, BS3 was added to the reaction in a final concentration of 5 mM. Then, the suspension was incubated for 30 min at room temperature and was

quenched subsequently by adding Tris-HCl pH 7.5 (final concentration 50 mM) and incubating the reaction for 15 min at room temperature. Then, protein lysate was added and the reaction was processed as described above.

**6 x Lämmli**

7 mL 4 x Tris-HCl/SDS pH 6.8  
3 mL glycerol  
1 g SDS  
1.2 mg bromphenolblue  
ad 10 mL ddH<sub>2</sub>O

**6 x Lämmli + DTT**

= 6 x Lämmli  
+ 930 mg DTT

**2.3.5 Biotinylation assay**

Biotinylation represents a commonly used method for detection of cell surface proteins [42]. 48 days after transfection, medium was removed from HEK293T cells which then were washed with PBS. Cell surface biotinylation was performed using 0.8 mM of non-cell permeable sulfo-NHS-SS-biotin (Pierce, Rockford) in PBS for 30 minutes at 4°C. The reaction was stopped with 10 mM glycine and the cells were transferred into fresh 50 mL Falcon tubes. After 2 wash steps with PBS (each time pelleting the cells by centrifugation at 4°C for 5 min at 1500 x g), the cell pellet was solubilised in 1 x lysis buffer with the proteinase inhibitor cocktail mix (see chapter 2.3.1). Then, biotinylated proteins were precipitated on Neutravidin agarose resin (Pierce) using 80 µL of neutravidin beads per reaction. First, beads were washed with 200 µL PBS and centrifuged after each wash step at 4°C for 1 min at 2500 x g. Biotinylated protein lysate (400 µg/reaction) was added to the washed beads and was rotated for 2 h at 4°C. Next, the suspension was washed 4 additional times with PBS containing 1 % NP-40 under the same centrifugation conditions as described above. Finally, elution was performed by adding 40 µL of elution buffer to the beads. Samples were incubated 10 min at 70°C before loading them on the SDS PAGE gel.

**Elution Buffer**

280 µL PBS  
40 µL 10 % NP-40  
80 µL 6 x Lämmli buffer + DTT

## 2.4 Förster resonance energy transfer (FRET)

FRET represents a commonly used tool for the analysis of molecular dynamics such like protein-protein interactions [43]. This method is based on the energy transfer between two fluorophores located in a defined spatial proximity to each other (Typically, less than 10 nm). Thereby, the emission spectrum of the first fluorophore (donor) is partially absorbed by the second fluorophore (acceptor) giving rise to a decrease in the emission spectrum of the donor and an increase of the acceptor emission spectrum. This spectral shift is finally measured as FRET signal. However, a prerequisite for a FRET signal is a spectral overlap of the donor and the acceptor. Based on this, for biological use the most commonly used pair of fluorophores is the combination of CFP as donor and YFP as acceptor. Interaction of proteins of interest can be studied by coupling them to these fluorophores, by coexpressing them in an appropriate cell line and by subsequent measurement of the FRET signal. In this study, FRET was used to analyse the assembly of CNGB1a subunits carrying the GV mutation with the CNGA1 subunit using following protocol:

HEK293 cells were transfected with CNGA1-CFP or soluble CFP (negative control) and wildtype or mutant YFP-CNGB1a. A CFP-YFP tandem construct served as FRET positive control [44]. Fluorescent images were captured 48-72 h after transfection on an Axioplan 2 microscope (Zeiss, Oberkochen, Germany) equipped with a Plan Neofluar 40 x objective (numeric aperture 0.75), a HMRc ccd camera and an AttoArc HBO100 mercury lamp illumination unit. Three fluorescent images per cell were collected using the CFP HC filter, YFP HC filter and FRET CFP-YFP HC filter sets (Semrock, Rochester). Fluorescence images were processed using the FRET plus macro (Zeiss) and the FRET efficiency was calculated as N-FRET using the method described by Xia and Liu [45].

## 2.5 Electrophysiological recordings

All experiments obtained from electrophysiological recordings in this study were performed by PD Dr. Xiangang Zong as described previously [25, 46, 47]. Maximal channel open probability ( $P_{max}$ ) was determined from the ratio of currents at saturating cGMP (1 mM) in the absence and the presence of 1  $\mu$ M  $Ni^{2+}$  as described previously [48, 49]. The following adjustments to the solutions were made for these experiments: KCl or NaCl with less than 0.01 ppm  $Ni^{2+}$  was used and HEPES concentration was lowered to 5 mM. EGTA / EDTA were omitted from the extracellular solution. The pipette solution contained 200 mM EDTA and 500 mM niflumic acid.

## 2.6 Statistics

All values are given as mean  $\pm$  S.E., and  $n$  is the number of experiments. An unpaired Student's  $t$  test was performed for the comparison between two groups. Values of  $p < 0.05$  were considered significant.

### 3 Results

#### 3.1 Splicing analysis of the c.3444+1G>A mutation in *CNGB1*

As described in chapter 1.5.2 the c.3444+1G>A splice site mutation in *CNGB1* has been associated with RP [32]. This mutation is located at the donor site of exon 32 and has been proposed to result in a frameshift and truncation of the last 28 amino acids (aa) of the corresponding protein. However, this ambiguous conclusion was not verified by experimental data. Therefore, the effects of c.3444+1G>A on splicing were reexamined by *in silico* and *in vitro* experiments.

##### 3.1.1 *In silico* splicing analysis of c.3444+1G>A

In order to reconstruct the mechanism by which c.3444+1G>A could lead to truncation of the last 28 aa of CNGB1a, *in silico* analysis was performed using the NNSplice 0.9 splice site prediction software ([http://www.fruitfly.org/seq\\_tools/splice.html](http://www.fruitfly.org/seq_tools/splice.html)) (Fig. 7). The DNA sequence used for this analysis starts with exon 32 and ends with the stop codon of *CNGB1*. A plausible explanation for the splicing scenario proposed by the original study would be the use of cryptic donor sites.

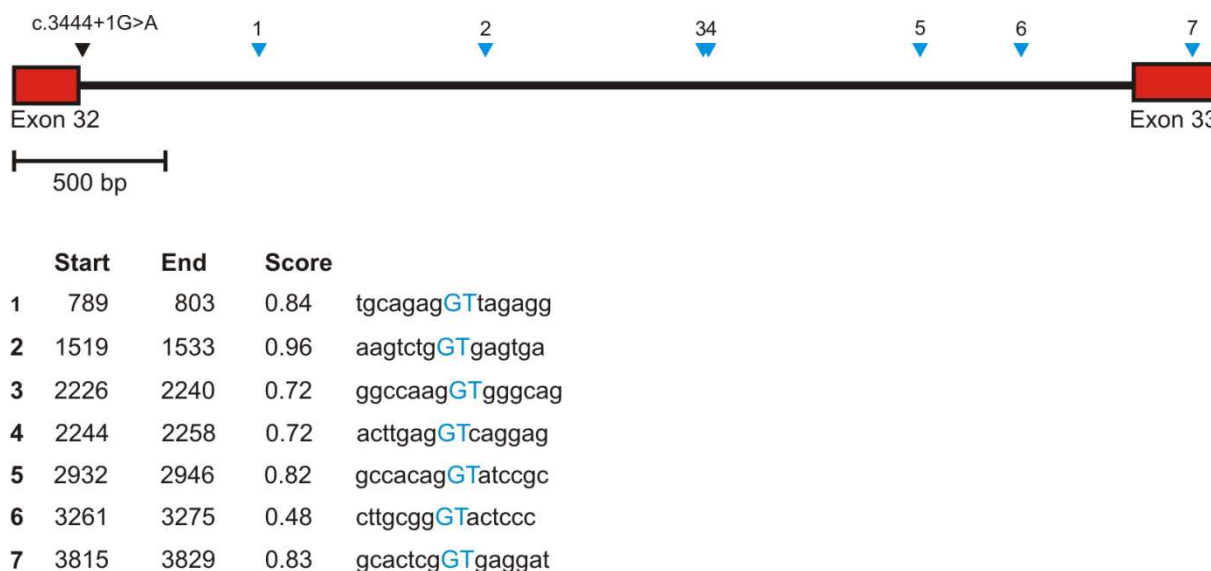


**Fig. 7 Donor site prediction of a *CNGB1* genomic DNA fragment encompassing exon 32-33 (3911 bp in length) using the NNSplice 0.9 splice site prediction software ([http://www.fruitfly.org/seq\\_tools/splice.html](http://www.fruitfly.org/seq_tools/splice.html)). The respective positions of the predicted donor sites on genomic DNA are shown as blue arrowheads, the position of the c.3444+1G>A mutation is marked by a black arrowhead. In the lower part of the figure, start and end positions of the DNA sequence flanking the donor site as well as the corresponding score values are shown. Donor site is highlighted in upper case (blue font).**

As shown in Fig. 7, the DNA sequence analysed herein harbours seven potential cryptic donor sites. Use of the cryptic donor site in exon 33 would indeed delete the sequence that encodes the last 28 aa. However, it would also lead to retention of intron 32. In this case, due to an intronic stop codon 171 bp after exon 32, the corresponding protein would lack all 97 aa encoded by exon 33.

### 3.1.2 Creation of wild type and mutant minigene constructs

In conclusion, no possible splice scenario could be reconstructed that would give rise to the deletion of only the last 28 aa of the CNGB1 protein. Therefore, the splicing of the construct containing the c.3444+1G>A mutation was analysed experimentally. For this purpose, a DNA fragment starting from the last 55 bp of intron 30 and ending with the last 42 bp after the stop codon within exon 33 of *CNGB1* was amplified by PCR from human genomic DNA and was sequenced. For cloning convenience, a 7.1 kb fragment of intron 31 flanked by *Xba*I sites was deleted. The final 6.4 kb minigene construct was subcloned into the pcDNA3 vector. The c.3444+1G>A mutation was inserted using standard site directed mutagenesis (Fig. 8).

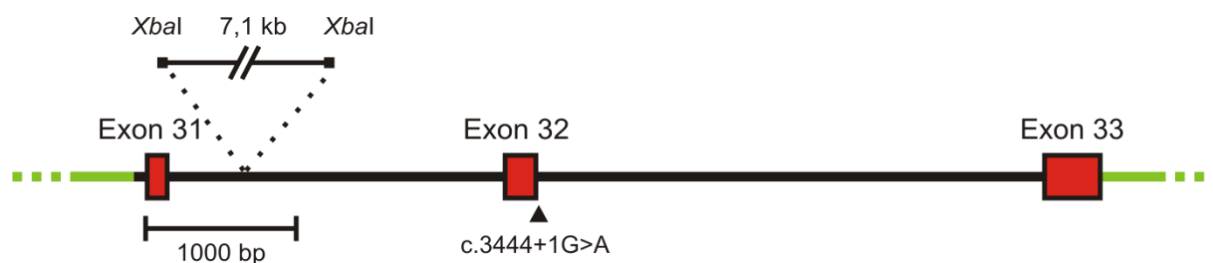


**Fig. 8 Schematic representation of the minigene construct used for the exon trapping experiment showing the position of the deleted intronic *Xba*I-fragment. pcDNA3 vector backbone sequence is depicted in green.**

### 3.1.3 Exon trapping experiments in HEK293T cells

Wild type and mutant minigene constructs were transfected in HEK293T cells and after 48 h, cells were harvested followed by total RNA isolation. After cDNA synthesis and PCR amplification with vector specific primers the splicing products derived from the minigenes were sequenced (Fig. 9).

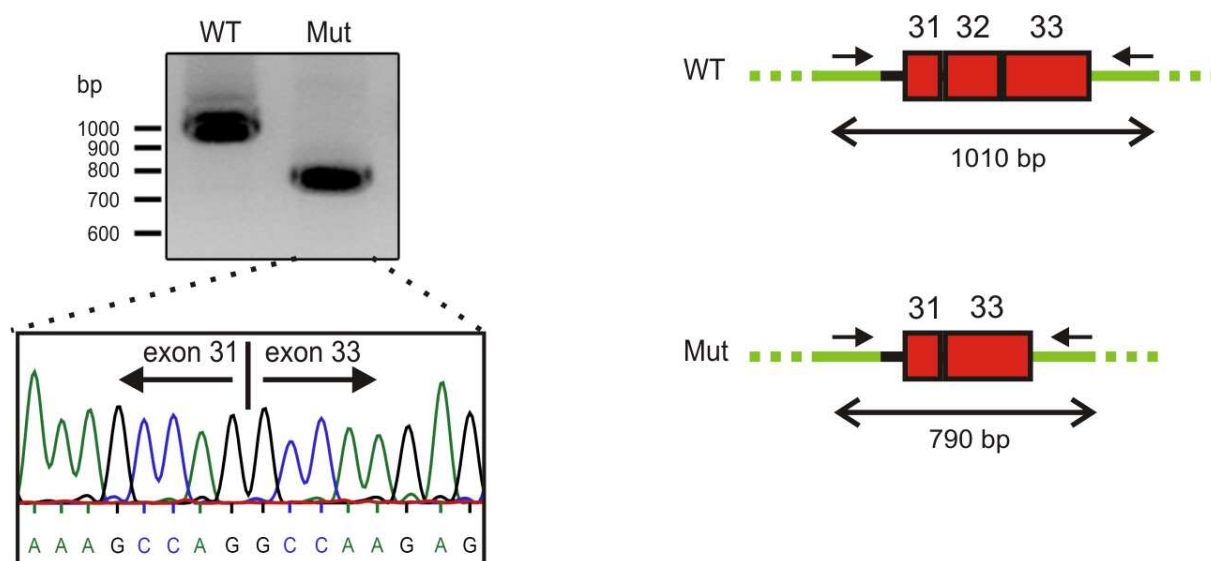


**Fig. 9 Exon trapping experiment from transfected HEK293T cells.** On the left, reverse transcriptase PCR from HEK293T cells transfected with mutant and wild type minigene constructs is depicted. The electropherogram for the c.3444+1G>A mutant shows the skipping of exon 32. Wild type construct was spliced correctly (data not shown). On the right, schematic representation of the splice products is shown. The length of the respective PCR products is indicated by double arrows. WT: wild type, Mut: c.3444+1G>A mutation.

As shown in the upper figure, the c.3444+1G>A mutation results in skipping of exon 32 thereby leading to a frameshift after exon 31. As a result, the regular coding region of CNGB1a stops after amino acid 1075 followed by 68 unrelated amino acids. The deleted part of CNGB1a encompasses 170 aa and covers the complete distal C-terminus including the last 10 aa of the  $\alpha$ C helix within the CNBD (Fig. 10).

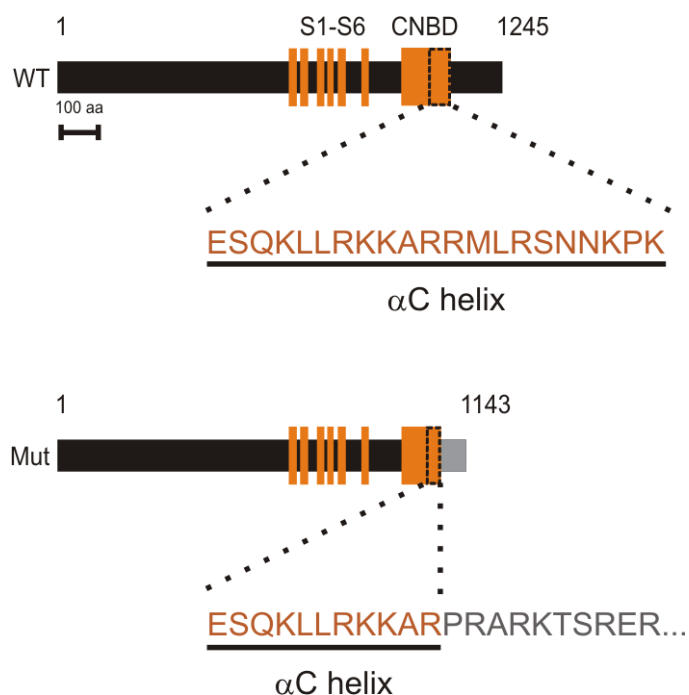


**Fig. 10 Schematic comparison of the WT and mutant protein demonstrating the lack of the entire distal C-terminus and the last 10 aa of the  $\alpha$ C helix in the context of the c.3444G>A mutation.** Skipping of exon 32 causes a frameshift which results in addition of 68 unrelated amino acids after aa position 1075 of the CNGB1a protein (highlighted in grey). The numbers represent the length of the respective proteins (1245 aa for WT and 1143 for the mutant). S1-S6: transmembrane segments.

### 3.1.4 *In vitro* expression of wild type and mutant rod CNG channels

To investigate the consequences of skipping of exon 32 on the full length protein the human full-length mutant CNGB1a was coexpressed in HEK293T cells with human CNGA1. The full-length mutant CNGB1a cDNA was obtained by deleting the exon 32 of the full-length wild type CNGB1 cDNA. For western blotting experiments membrane proteins were isolated from HEK293T cells transfected with CNGA1 and wild type or mutant CNGB1a.

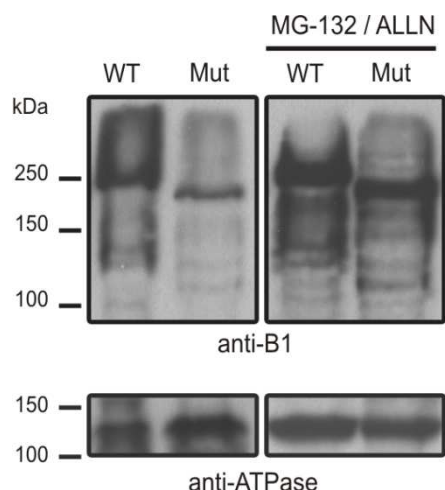


**Fig. 11 Western blot of membranes isolated from HEK293T cells transfected with CNGA1 and wild type or mutant CNGB1a probed with anti-B1 (top panel) or anti-ATPase (bottom panel).** The weaker expression of the mutant protein was normalized in the presence of the proteasome inhibitors MG-132 and ALLN. The blot was probed with an antibody directed against the N-terminus of CNGB1a (PPc6N, [23]). As loading control anti-ATPase antibody (1:1000, clone  $\alpha$ 6F, developed by D.M. Fambrough, obtained from the Developmental Studies Hybridoma Bank, Iowa) was used. In proteasome inhibition experiments MG-132 and ALLN (25  $\mu$ M each, Calbiochem) were added directly to the cells sixteen hours prior to harvesting.

As shown in Fig. 11, in the western blot analysis using an antibody directed against the N-terminus of CNGB1a the expected 240 kDa band for the wild type CNGB1a could be detected. As anticipated, the mutant CNGB1a protein was smaller than the wild type counterpart. Furthermore, the expression level of the mutant CNGB1a was considerably reduced compared to the wild type CNGB1a. Since this difference in expression could be reversed by the addition of the proteasome inhibitors MG-132 and ALLN, respectively, the conclusion can be drawn that the mutant protein is partially degraded by the proteasome.

In summary, the c.3444+1G>A mutation was shown to result in skipping of exon 32 on mRNA level thereby leading to a frameshift after exon 31 and a premature stop codon. On protein level this mutation gives rise to deletion of the last 170 aa of the mutant protein including 10 aa of the  $\alpha$ C helix within the CNBD. Finally, *in vitro* results from HEK293T cells after coexpression of the mutant CNGB1a with CNGA1 have shown that the mutant CNGB1a is prone to proteasomal degradation.

## 3.2 Functional analysis of the G993V mutation in *CNGB1*

As described in chapter 1.7, this part of the study addressed the role of the CNGB1a subunit on the activation process of the heteromeric rod CNG channel. For this purpose, a naturally occurring point mutation in the human *CNGB1* gene that leads to a glycine-valine exchange at position 993 in the CNBD of CNGB1a (CNGB1aGV) was analysed. This mutation was identified in a French family suffering from retinitis pigmentosa (RP) [31].

### 3.2.1 *In silico* analysis

To examine the effects of the G993V mutation computationally, two approaches were performed. The first approach included the analysis of the evolutionary conservation of the glycine residue at position 993 among different proteins known to have very similar cyclic nucleotide-binding domain structure (see chapter 1.4.1). In the second approach, to analyse the consequences of the GV mutation on the conformation of the CNBD in CNGB1a, a molecular dynamics (MD) simulation was performed by the group of Prof. Wanner, Department of Chemistry, Ludwig Maximilians Universität München (Fig. 12). As template coordinates the crystal structure of the CNBD of the sea urchin HCN channel was used [50].

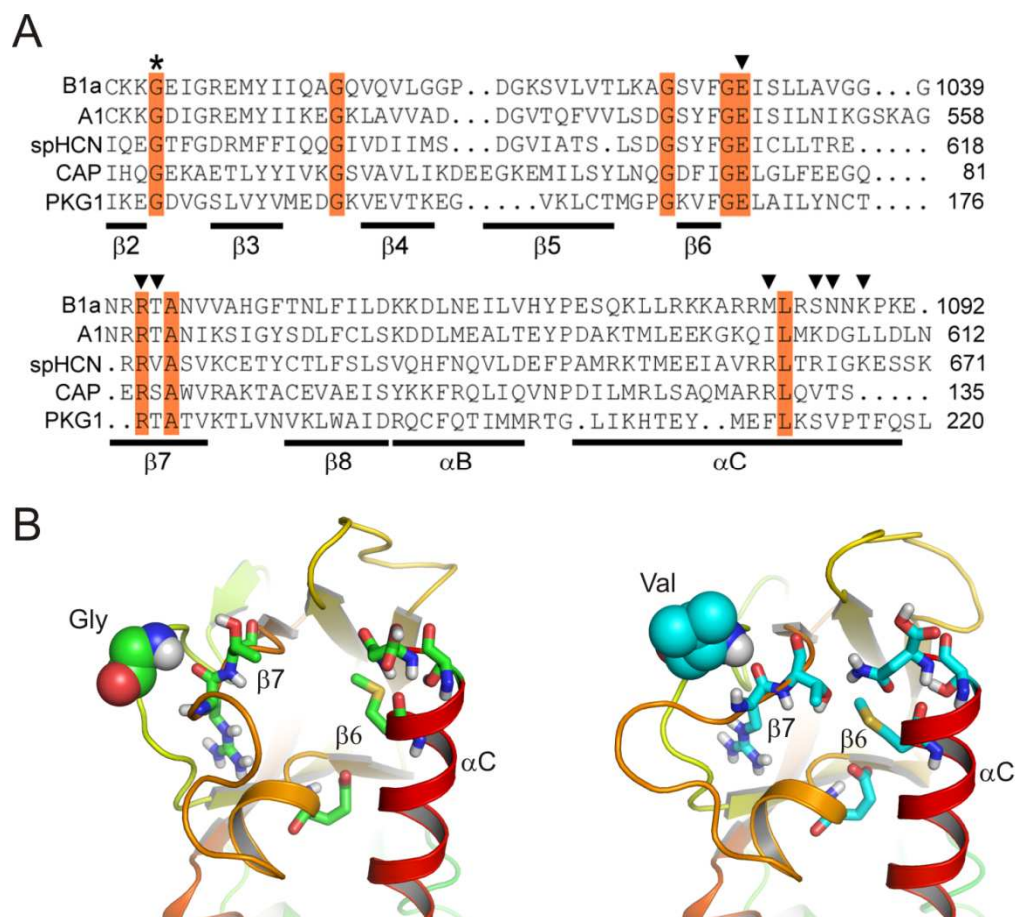


**Fig. 12 *In silico* analysis of the G993V mutation.** A) Sequence alignment of the  $\beta$ 2- $\alpha$ C region of the CNBD of human CNGB1a, human CNGA1, *E. coli* CAP, sea urchin (sp) HCN1 and human PKG1. Invariant residues are highlighted in red. The invariant glycine residue within the  $\beta$ 2- $\beta$ 3 loop that is mutated to valine (GV mutation) in the CNGB1a subunit of RP patients is marked with an asterisk. Residues identified in the crystal structure of HCN channel CNBDs to participate in cyclic nucleotide-binding [51] are marked with arrowheads. B) Predicted structure of the cGMP binding pocket of CNGB1a (left) and CNGB1aGV (right). The sequences were threaded onto the crystal structure of the CNBD of spHCN [51] by using Modeller [52] and analysed using molecular dynamics simulations. The glycine and the valine residue in the  $\beta$ 2- $\beta$ 3 loop of CNGB1a and CNGB1aGV, respectively, are represented as space filling spheres. Residues in the  $\beta$ 6 and  $\beta$ 7 strands as well as in the C helix participating in cGMP-binding are shown as sticks. Only one monomer is shown for clarity.

As outlined in Fig. 12, the GV mutation in the CNBD of CNGB1a refers to a glycine residue in the  $\beta$ 2- $\beta$ 3 connecting loop that is strictly conserved throughout evolution. The available crystal structures of CNBDs indicate that the glycine is not directly involved in cGMP binding but that it is essential for the integrity of the overall fold of the CNBD [53]. As is evident from Fig. 12, the GV mutation induces major structural alterations in the CNBD. These rearrangements lead to the occlusion of the cGMP binding cavity and a reduction of the cGMP binding site volume.

### 3.2.2 Expression of CNGA1GV

Based on the findings from the *in silico* analysis, the GV mutation could have the potential to impair cGMP binding and, hence, channel activation. To test this hypothesis the GV mutation was introduced into the CNBD of CNGA1 and the expression as well as the electrophysiological properties of the mutant CNGA1 were analysed (Fig. 13).

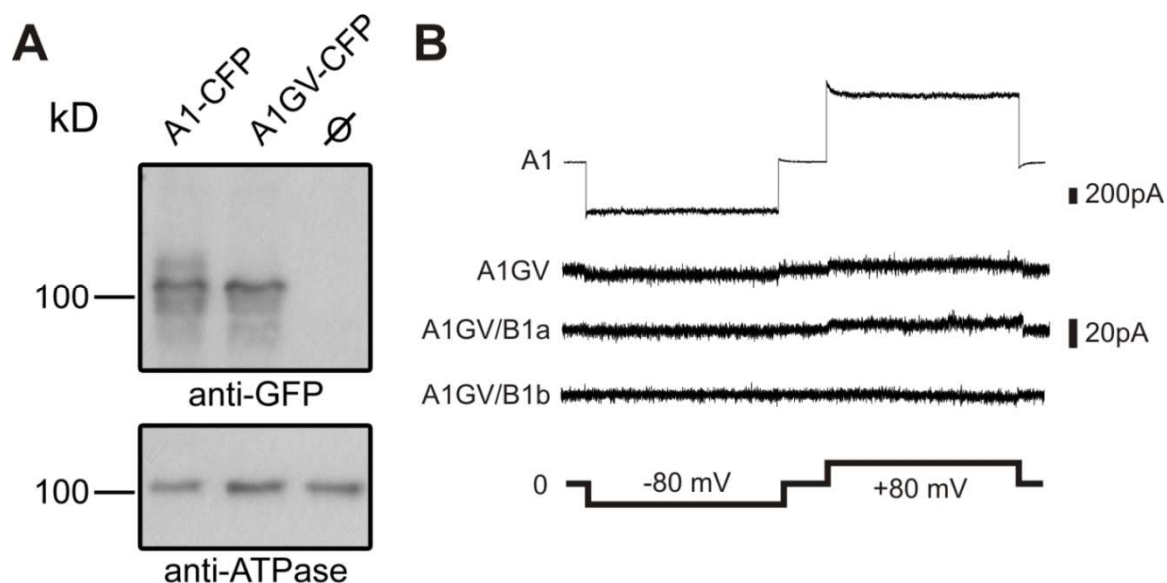


**Fig. 13 CNGA1GV is expressed on the plasma membrane of transfected HEK293 cells.** A) Top panel: Western blot of membranes from HEK293 cells transfected with CNGA1-CFP or CNGA1GV-CFP, respectively. The blot was probed with anti-GFP antibody. Bottom panel: membranes probed against the ATPase  $\alpha$  subunit. (B) Representative current traces elicited by 1 mM cGMP and voltage steps (2 s each) to -80 mV and +80 mV in excised patches from HEK293 cells expressing CNGA1 (A1), or CNGA1GV (A1GV), CNGA1GV/CNGB1a (A1/B1a) and CNGA1GV/CNGB1b (A1/B1b).

As shown in Fig. 13, the GV mutation had no consequences on protein expression level. However, as predicted, CNGA1GV channels were functionally inactive even in the presence of 1 mM cGMP. Coexpression of CNGB1a or the olfactory CNGB1b subunit that lacks the GARP domain failed to rescue channel activity.

### 3.2.3 Electrophysiological measurements of heteromeric CNGA1/CNGB1aGV channels

Next step was to analyse the effects of the GV mutation in CNGB1a on the heteromeric channel complex. To this end, CNGA1 was coexpressed together with either wild type or mutant CNGB1a and the properties of the resulting currents were compared to currents induced by CNGA1 alone (Fig. 14).

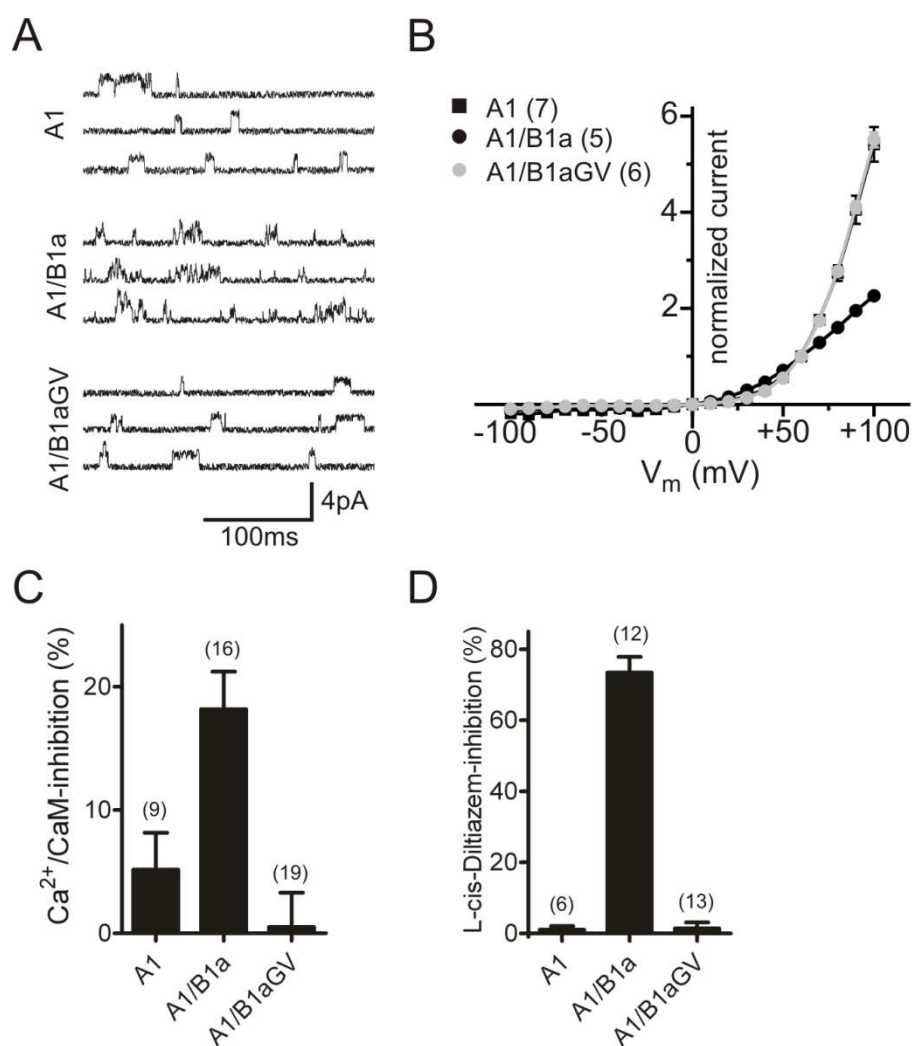


**Fig. 14 Electrophysiological characterisation of heteromeric CNGA1/CNGB1aGV channels.** Single-channel currents induced at +60 mV by 3  $\mu$ M cGMP in excised patches of HEK293 cells transfected with CNGA1 (A1), CNGA1/CNGB1a (A1/B1a) or CNGA1/CNGB1aGV (A1/B1aGV). (B) Current-voltage relation of A1, A1/B1a and A1/B1aGV in the presence of 2 mM Ca<sup>2+</sup> and 1 mM Mg<sup>2+</sup> in the extracellular solution. Current was normalized to the current at +60 mV. (C) Inhibition of A1, A1/B1a and A1/B1aGV currents by 100  $\mu$ M Ca<sup>2+</sup> / 250 nM calmodulin in the bath solution. Currents were induced at +80 mV by 100  $\mu$ M cGMP. (D) L-cis-diltiazem (10  $\mu$ M) block of A1, A1/B1a and A1/B1aGV currents induced by 300  $\mu$ M cGMP at +80 mV. Number of experiments is given in brackets.

Surprisingly, currents obtained after coexpression of CNGA1 and CNGB1aGV did not exhibit typical CNGB1a-mediated features but were indistinguishable from currents of homomeric CNGA1 channels (Fig. 14 A-D). While single channel currents of heteromeric CNG channels are characterised by very brief open-closed transitions (single channel flicker), single channel currents obtained after coexpression of CNGA1 and CNGB1aGV displayed long openings which is typical of homomeric CNGA1 channels (Fig. 14 A). In addition, the strong outwardly-rectifying current-voltage relation of channels obtained after coexpression of CNGA1 and CNGB1aGV in the presence of extracellular divalent ions was virtually identical to that of the homomeric CNGA1 channel, but clearly differed from that of weakly rectifying wild type heteromeric channels (Fig. 14 B). In contrast to wild type CNGB1a, CNGB1aGV did not increase  $Ca^{2+}$ /CaM sensitivity if coexpressed with CNGA1 (Fig. 14 C). Probably the most indicative feature resulting from the presence of the CNGB1 subunit is the generation of a high affinity site for block by L-cis-diltiazem [26]. Indeed, unlike homomeric CNGA1 channels, heteromeric CNGA1/CNGB1a channels were efficiently blocked by this drug. By contrast, currents obtained after coexpression with CNGB1aGV were not sensitive to L-cis-diltiazem (Fig. 14 D).

### 3.2.4 Coassembly and cell surface expression of CNGA1/CNGB1aGV heteromers

The total absence of CNGB1a-mediated properties in conjunction with the complete correspondence with the biophysical properties of homomeric CNGA1 currents indicated that currents measured after cotransfection of CNGA1 and CNGB1aGV were purely caused by CNGA1 homomers. A possible explanation for this result would be that after cotransfection of CNGA1 and CNGB1aGV only homomeric CNGA1 channels are present in the membrane because CNGA1/CNGB1aGV heteromers are not assembled, are rapidly degraded or fail to be transported to the plasma membrane. To test these options, biotinylation, co-immunoprecipitation and FRET experiments on CNGA1/CNGB1aGV heteromers were performed (Fig. 15).

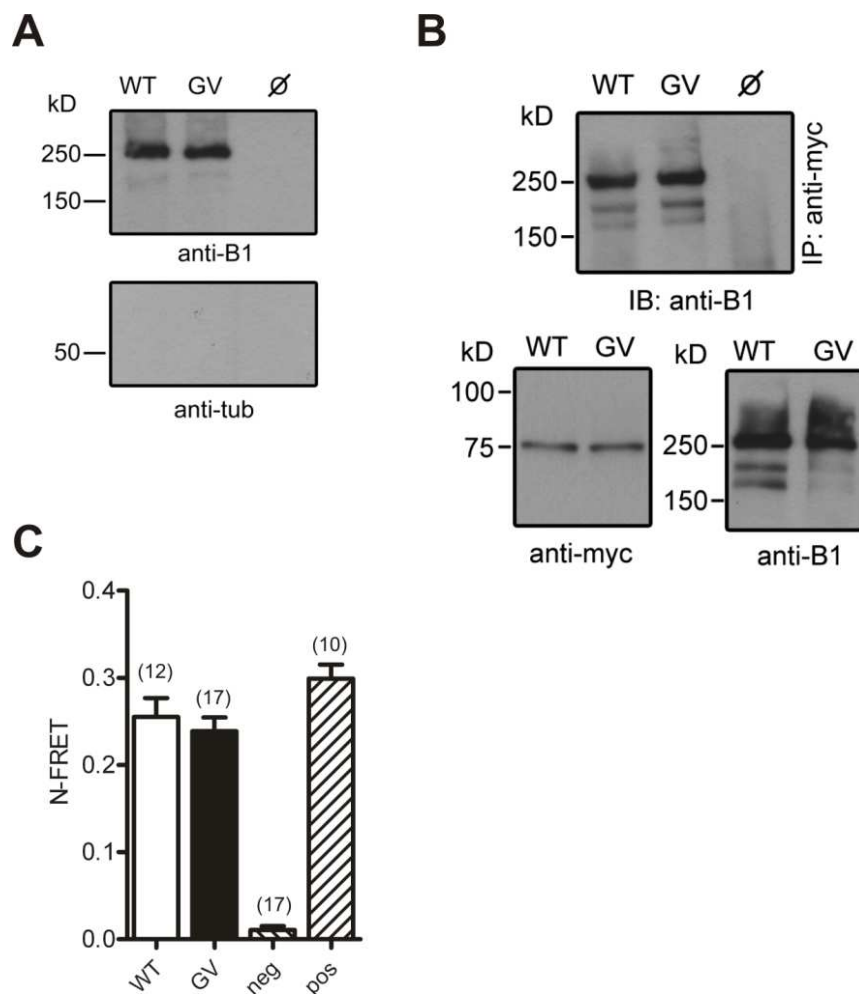


**Fig. 15 Cell-surface expression and assembly of CNGA1/CNGB1GV heteromers.** A) Biotinylation of non-transfected ( $\emptyset$ ), CNGA1/CNGB1a (WT) and CNGA1/CNGB1aGV (GV) transfected HEK293 cells probed with anti-B1 (top panel) or anti-tubulin (tub, bottom panel) antibodies. B) Co-immunoprecipitation (co-IP) from lysates of HEK293 cells co-transfected with myc-tagged CNGA1 and wild type CNGB1a or CNGB1aGV, respectively. Top panel: immunoprecipitation (IP) using anti-myc for pulldown and anti-B1 for detection. Bottom panel: Western blots showing the starting material for the co-IP probed with anti-myc (left) or anti-B1 antibodies (right). C) N-FRET ratios calculated from HEK293 cells co-transfected with CNGA1-CFP and YFP-CNGB1a (WT) or YFP-CNGB1aGV, respectively. HEK293 cells transfected with CFP and YFP-CNGB1a or a CFP-YFP tandem were used for the calculation of negative (neg) and positive (pos) control N-FRET values, respectively. Number of experiments is given in brackets.

As is evident from Fig. 15 A, cell surface biotinylation experiments using membrane impermeable amine-reactive biotin showed that both wild type and mutant channels were present at the membrane of transfected cells. In addition, CNGB1aGV could be co-immunoprecipitated with CNGA1 indicating the formation of stable heteromers (Fig. 15 B). Finally, assembly of CNGA1 with CNGB1aGV was also verified by Förster resonance energy transfer (FRET) (Fig. 15 C).

### 3.2.5 Identification of inhibitory domains in CNGB1a

Another explanation for the selective detection of homomeric CNGB1a currents in HEK293 cells transfected with CNGB1a and CNGB1aGV may be that homomeric and mutant heteromeric CNGB1 channels do coexist in the plasma membrane but in contrast to homomeric CNGB1 channels mutant heteromers cannot be activated by cGMP and, thus, do not contribute to any measurable current. In an attempt to identify structural determinants conferring an inhibitory action of CNGB1aGV the GV mutation was introduced into the olfactory CNGB1b subunit that differs from CNGB1a by lacking the GARP domain. This new mutant was coexpressed with CNGB1a and patch clamp recordings were performed (Fig. 16).

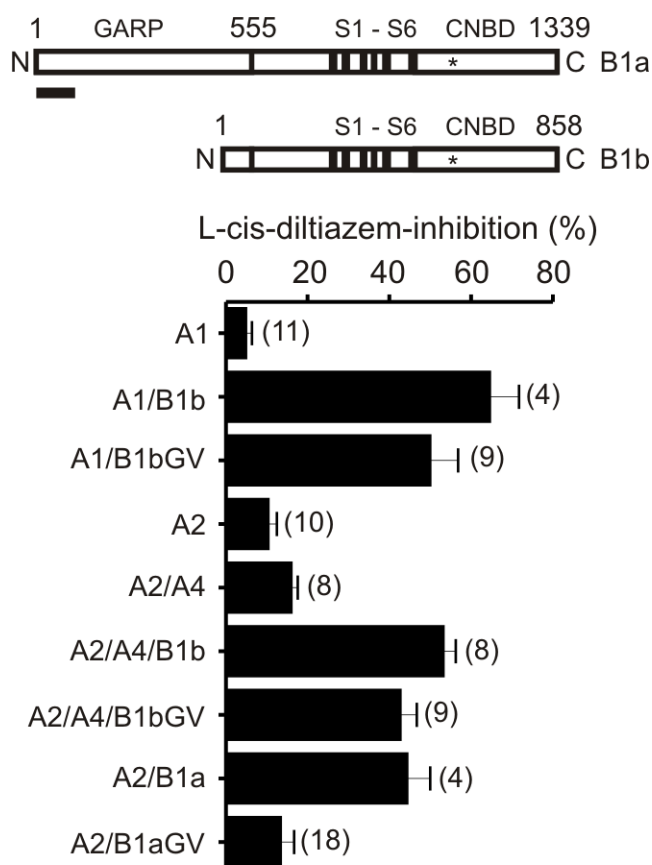


**Fig. 16 Identification of N-terminus of CNGB1a (herein referred to as “GARP domain”) as the inhibitory domain.** The GV mutation does not impair channel function in the context of the olfactory CNGB1b isoform lacking the GARP domain. Top panel: Schematic representation of CNGB1a and CNGB1b subunits. The position of the GV mutation is highlighted by an asterisk. Amino acid position 555 is highlighted since starting from this position CNGB1a and CNGB1b are identical. Bottom panel: Summary graph showing the L-cis-diltiazem sensitivity of various homo- or heteromeric channels. Currents were elicited by 300  $\mu$ M cGMP at +80 mV. L-cis-diltiazem was used at 50  $\mu$ M for A2, A2/A4, A2/A4/B1b and A2/A4/B1bGV and at 10  $\mu$ M for all other channels. S1-S6, transmembrane domains; CNBD, cyclic nucleotide-binding domain. Scale bar marks 100 amino acids.

Surprisingly, as shown in Fig. 16, L-cis-diltiazem sensitive currents were now obtained with both wild type and mutant CNGB1b subunits. Sensitivity to L-cis-diltiazem was also consistently observed when the GV mutation was introduced into the native olfactory CNG channel complex consisting of CNGA2/CNGA4 and CNGB1b. Like for CNGA1 the wild type but not the mutant CNGB1a subunit induced L-cis-diltiazem sensitivity when coexpressed together with CNGA2. These results indicated that the GARP domain mediates the dominant negative effect of CNGB1aGV. To identify the inhibitory determinants within the GARP domain, a systematic mutation screening was performed by deleting specific regions of this domain. The respective constructs were coexpressed with CNGA1 in HEK293 cells followed by electrophysiological measurements of L-cis-diltiazem mediated CNG current inhibition. Fig. 17 shows a summary of the most important mutation constructs analysed in this approach.

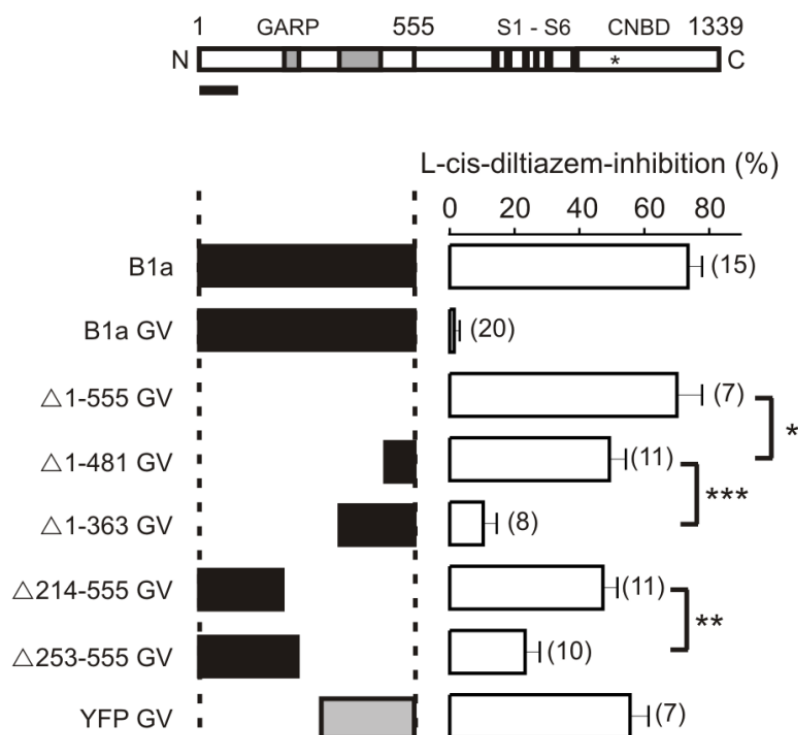


**Fig. 17 Mutagenesis screen within the GARP domain.** Top panel: cartoon showing the CNGB1a subunit. The two sequences conferring most of the inhibitory effect are highlighted in grey. Bottom panel: graphic overview on N-terminal truncation constructs (left) and summary graph comparing the effect (% inhibition) of 10  $\mu$ M L-cis-diltiazem on cGMP currents (300  $\mu$ M, +80 mV, right) measured from HEK293 cells co-transfected with CNGA1 and various N-terminal truncated CNGB1aGV mutants or a B1aGV chimera in which the N-terminus was replaced by the yellow fluorescent protein (YFP). Number of experiments is given in brackets. \* =  $p < 0.05$ , \*\* =  $p < 0.01$ , \*\*\* =  $p < 0.005$ . Scale bar marks 100 amino acids. S1-S6, transmembrane helices.

As is evident from Fig. 17, study of mutants with deletions in the GARP domain identified two regions (residues 214-253 and 364-481) of CNGB1a that confer most of the inhibitory effect. Fusion of an unrelated peptide (YFP) to the N-terminus of CNGB1bGV did not result in channel inhibition excluding unspecific effects which could be mediated merely by the length of the N-terminal domain.

As described in chapter 2.1.12, the experiments shown so far were obtained using rat CNGB1a and bovine CNGA1 channels. To examine if inhibitory effects of the GARP domain can be obtained using CNG channels from other species, the GV mutation was introduced into the human CNGB1a (hCNGB1a) subunit containing and lacking the GARP domain. After coexpression with human CNGA1 (hCNGA1), L-cis-diltiazem sensitivity was measured for these channels. The results are shown in Fig. 18.

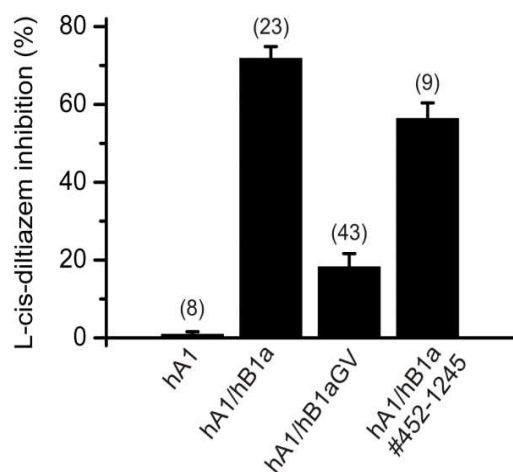


**Fig. 18 Effects of the GV mutation and of the GARP domain on human rod CNG channels.** Percent inhibition by 10  $\mu$ M L-cis-diltiazem of currents obtained after cotransfection of human CNGA1 with wild type or mutant human CNGB1a lacking or containing the GARP domain in presence of 300  $\mu$ M cGMP. hB1a#452-1245 corresponds to the rat CNGB1a construct B1a#556-1339 (see i.e. Fig. 17 and Fig. 19). Number of experiments is shown in brackets.

As shown in Fig. 18 the GV mutation as well as the GARP domain of the human rod channels show very similar electrophysiological characteristics regarding the L-cis-diltiazem sensitivity as described above for rat CNGB1a and bovine CNGA1 channels, respectively. This indicates that the observed effects of the GARP domain represent a general mechanism transferable to rod channels of all species.

### 3.2.6 Coexpression of GARP as soluble protein

To test whether the GARP domain can act inhibitory as an autonomous protein it was coexpressed as separate protein (B1a#1-555) together with CNGA1 and a CNGB1a truncation construct (B1a#556-1339, see cartoon in Fig. 19 A).

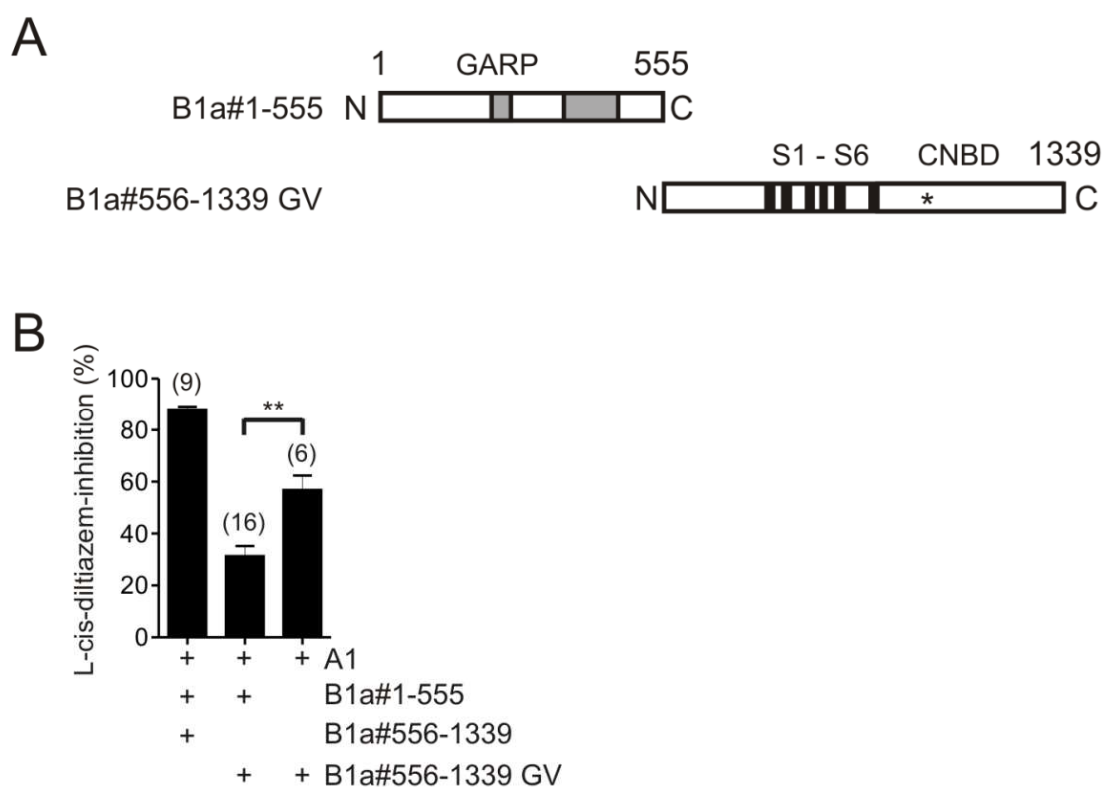


**Fig. 19 GARP acts as an autonomous unit when coexpressed as soluble protein.** A) Schematic representation of the truncated B1a#556-1339 GV channel and the protein corresponding to the GARP domain. B) Percent inhibition by 10  $\mu$ M L-cis-diltiazem of currents obtained after cotransfection of CNGA1 with various CNGB1a-derived constructs as indicated. Number of experiments is given in brackets. \*\* =  $p < 0.01$

Currents obtained from the coexpression of CNGA1 with B1a#556-1339 were sensitive to L-cis-diltiazem. By contrast, coexpression of the GARP domain, CNGA1 and CNGB1a#556-1339GV again abolished the block by L-cis-diltiazem (Fig. 19 B). This finding suggested that the GARP domain exerts its inhibitory effect even if it is not covalently linked to the CNGB1 core.

To test if the inhibitory effect of GARP is mediated by direct binding of this domain to the CNGB1a or CNGA1 subunit, co-immunoprecipitation experiments were performed (Fig. 20).

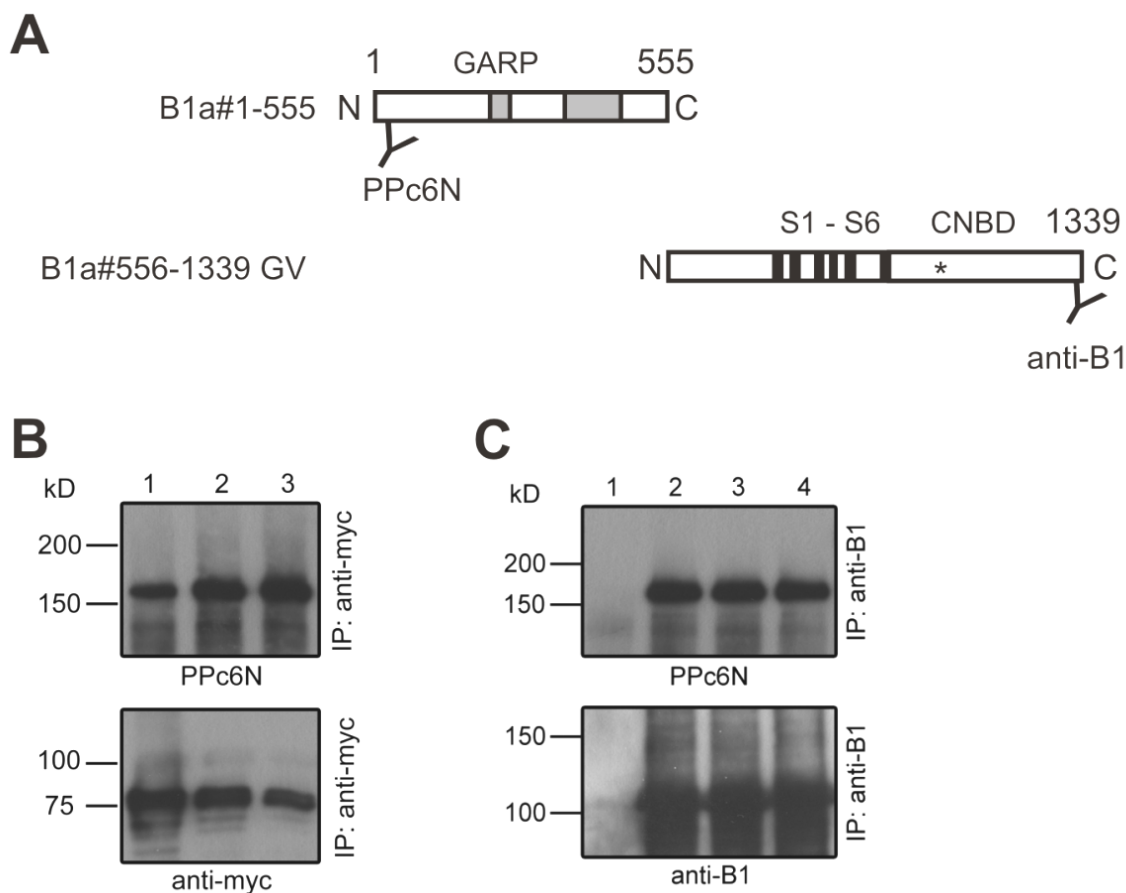


**Fig. 20 Co-immunoprecipitation of the GARP domain (B1a#1-555) with CNGA1 (myc-tagged) or CNGB1a#556-1339 WT or GV.** A) Schematic representation of the truncated B1a#556-1339 GV channel and the protein corresponding to the GARP domain (B1a#1-555) and binding sites of the B1a-specific antibodies used for experiments shown in B and C, respectively. B) Co-IP using the anti-myc antibody capable of the immunoprecipitation of myc tagged CNGA1 C) Co-IP using anti CNGB1 directed against the C-terminus of this protein.

1, coexpression of A1 + B1a#1-555; 2, A1 + B1a#1-555 + B1a#556-1339; 3, A1 + B1a#1-555 + B1a#556-1339GV; 4, B1a#1-555 + B1a#556-1339. Anti-B1, rabbit polyclonal antibody directed against the C-terminus of CNGB1a. PPc6N, rabbit polyclonal antibody directed against the N-terminus of CNGA1. IP, immunoprecipitation.

As is evident from Fig. 20 B and C, the soluble GARP domain formed stable protein complexes with both CNGA1 and either mutant or wild type CNGB1a#556-1339. Therefore, the inhibitory action of GARP on the channel is probably due to direct binding of this domain to the channel core.

### 3.2.7 Role of a functional CNBD of CNGB1 for CNG channel activation

Results shown in Fig. 20 indicate that the GARP domain binds to both CNGA1 and CNGB1 subunits in the heteromeric CNG channel complex. In wild type heteromers the identified GARP-channel interaction does not interfere with cGMP-dependent activation. By contrast, in the presence of the GV mutation the GARP domain completely shuts down channel activity. Based on MD simulations (Fig. 12) the conclusion can be drawn that the inhibitory effect of GARP may be causally linked to the inability of CNGB1aGV to bind cGMP. To test this hypothesis the effects of GARP in the presence of a double mutation in the  $\beta$ 7 strand of the CNBD (R1042E and T1043A, herein after referred to as RT>EA) that is well known to abolish cyclic nucleotide-binding in CNG and HCN channels [13, 51] were analysed (Fig. 21).

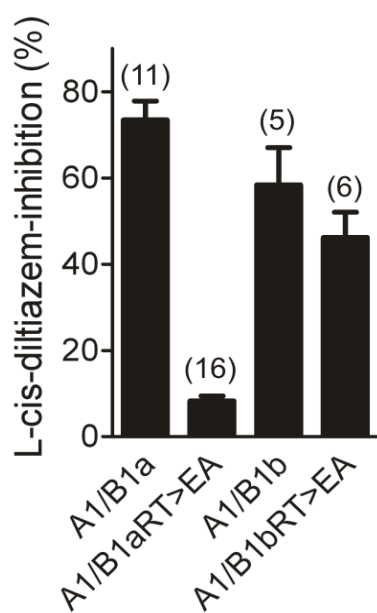


**Fig. 21 Summary graph comparing the L-cis-diltiazem sensitivity of heteromeric channels containing wild type and cyclic nucleotide-binding deficient (RT>EA) B1a or B1b subunits.** RT>EA: substitution of arginine and threonine within the  $\beta$ 7-sheet of the CNBD by glutamate and alanine, respectively. Number of experiments is given in brackets.

As anticipated, in the backbone of CNGB1b the double mutation did not interfere with the formation of functional heteromeric (L-cis-diltiazem sensitive) channels. However, when introduced into CNGB1a the mutation fully blocked heteromeric channel activity and only the residual homomeric (L-cis-diltiazem insensitive) CNGA1 channel was detected (Fig. 21). Thus, with respect to its functional effect on heteromeric channels containing or lacking the GARP domain, the RT>EA mutation was indistinguishable from the GV mutation.

### 3.2.8 Opening probability of channels containing or lacking the GARP domain

The experiments shown so far indicated that the GARP domain blocks gating of heteromeric CNG channels which contain a CNGB1 subunit deficient for cGMP binding. The next question was whether the GARP domain could also interfere with the gating of wild type heteromeric channels containing a functional CNBD. If so, differences in some electrophysiological parameters should also be detectable when comparing wild type CNGA1/CNGB1a with CNGA1/CNGB1a#556-1339 channels lacking GARP. To test one of these parameters, cGMP sensitivity for both channel types was measured but no apparent differences were detectable in this experiment (data not shown). However, the analysis of the maximal open probability for cGMP ( $P_{\max}$ ) showed that heteromeric channels containing the GARP domain had a significantly lower  $P_{\max}$  compared to channels lacking this domain (Fig. 22).

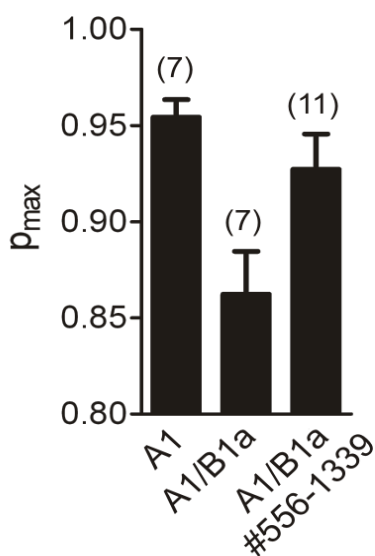


**Fig. 22 Summary graph comparing the maximal open probability for cGMP ( $P_{\max}$ ) of wild type homomeric A1, heteromeric A1/B1a and A1/B1a#556-1339 channels.** ( $P_{\max(\text{cGMP})}$ : CNGA1/CNGB1a =  $0.86 \pm 0.02$  (n=7), CNGA1/CNGB1a#556-1339 =  $0.93 \pm 0.02$  (n=11),  $p < 0.05$ ).

The finding that the presence of the GARP domain lowers the opening probability of CNG channels strongly supports the notion that the GARP domain acts as gating inhibitor in the rod photoreceptor channel.

Based on the results described in chapters 3.2.1-3.2.8, a final model was worked out in order to explain the observed effects (Fig. 23).

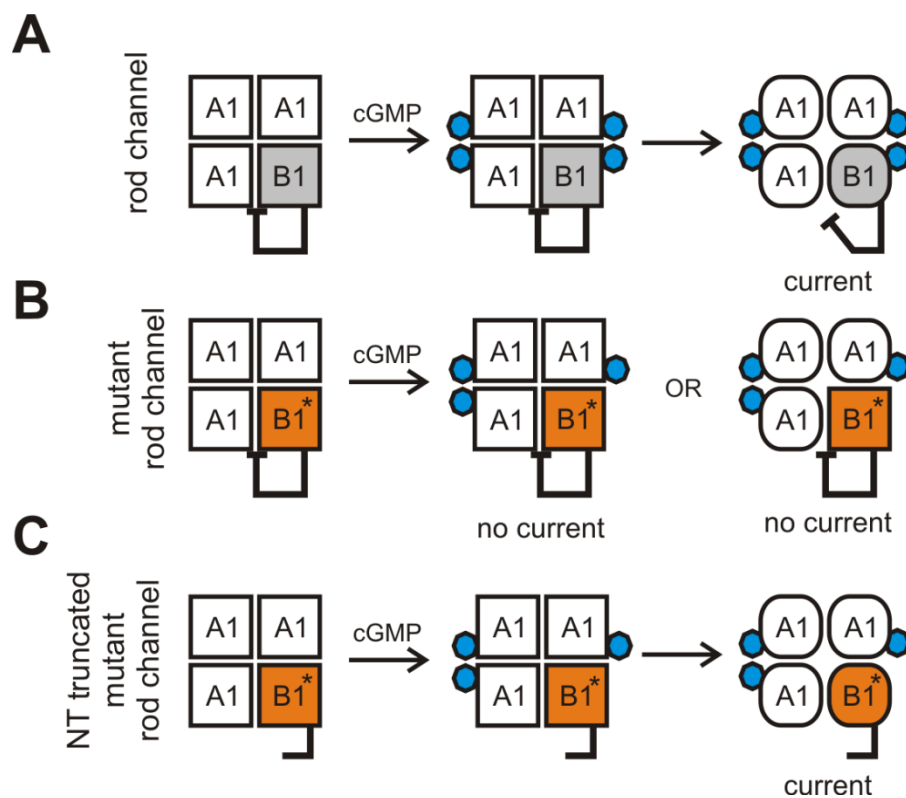


**Fig. 23 Model of the action of the GARP domain in wild type and mutant heteromeric CNG channels.** A) In wild type rod channels, GARP domain serves as a gating inhibitor. Binding of cGMP to CNGB1a subunit releases the tonic inhibition mediated by the GARP domain giving rise to channel opening. For reasons of clarity, the conceivable intermediates (i. e. if only one or two cGMP are bound to CNGA1) are not included in this model. B) GV mutation in CNGB1a probably prevents cGMP binding to this subunit. Therefore, the tonic inhibition of GARP may not be released and the channels remain in the closed state. C) If the GARP domain is removed from the mutant CNGB1 subunit the heteromeric channels are able to open in the presence of cGMP for two reasons. The first reason is the fact that binding of two cGMP was shown to be sufficient for maximal opening of olfactory CNG channels (see chapter 1.4.2). The second reason is the absence of the GARP domain as gating inhibitor.

The final conclusion that can be drawn from the model shown in Fig. 23 is that binding of cGMP to the CNGB1a subunit serves as a prerequisite for opening of rod CNG channels because of the inhibitory effect of the GARP domain on the gating process.

## 4 Discussion

### 4.1 Splicing analysis of the c.3444+1G>A mutation in *CNGB1*

In this part of the study, the pathogenic effect of a previously reported splice site mutation in *CNGB1* could be verified experimentally. Initial *in silico* analysis suggested that no splicing scenario would lead to “a frameshift and truncation of the last 28 aa” of CNGB1a as postulated by the original study [32]. Using *in vitro* exon trapping experiments it could be shown that this mutation gives rise to skipping of exon 32. However, due to the limitation of exon trapping experiments, the possibility that in photoreceptors the mutation may have other effects on splicing cannot be completely excluded.

Based on the results obtained in HEK293T cells in this study, the c.3444+1G>A mutation may lead to the RP phenotype by negatively affecting the

i) Channel expression. The expression of the mutant CNGB1a is compromised by the action of the proteasome. This may also be the case in rod photoreceptors resulting in reduction or in complete loss of channel. Mutations that result in premature stop codons are known to trigger nonsense mediated mRNA decay (NMD) [54]. Since skipping of exon 32 gives rise to a premature stop codon, it seems possible that c.3444+1G>A mutant transcripts are affected by NMD *in vivo*, which would also negatively affect channel expression.

(ii) Channel targeting. Recently, it has been shown that the distal C-terminus of CNGB1a contains an ankyrin G binding motif responsible for the proper targeting of the channel to rod outer segments [17]. This domain is located within the deleted sequence in the mutant CNGB1a. Thus, if the channel is expressed, its targeting to rod outer segments may be affected by the mutation.

(iii) Channel function. It has been shown that the structural integrity of the  $\alpha$ C helix of the CNBD is crucial for proper channel gating [48, 55, 56]. Since the c.3444+1G>A mutation results in loss of the last 10 aa of the  $\alpha$ C helix, the mutant channel, even if expressed at normal levels in rod outer segments, would be most probably non-functional. Which of these parameters (and to which extent) contributes to the disease in affected patients remains to be determined.

A comparison of the clinical investigations performed on patients which are affected by the c.3444+1G>A mutation with those affected by the c.2978G>T (p.G993V) mutation would be helpful in order to gain some insights into functional consequences of these two mutations *in vivo*. However, since clinically relevant parameters (i. e. electroretinogram) were examined only for one patient in the respective studies [31, 32], this comparison appears to be rather unreasonable at this point.

## 4.2 Functional analysis of the G993V mutation in *CNGB1*

In this part of the study the role of the CNGB1a subunit in the cGMP-dependent activation process of the rod photoreceptor CNG channel was examined. The CNBD of CNGB1a contains all canonical residues required for high affinity cGMP binding [26, 47, 57-59] and was shown in photoaffinity labeling experiments to bind cGMP [60]. While these findings suggest that CNGB1a contributes to channel activation, the analysis of the role of CNGB1a in this process has been hampered by the fact that CNGB1a does not form functional homomeric channels. The results of this study have shed new light on this issue by analyzing a naturally occurring mutation in CNGB1a of RP patients (GV mutation) that impairs the structural integrity and/or cGMP binding capability of the CNBD. It was found that this mutation exerts a strong dominant negative effect leading to a complete functional silencing of heteromeric channels. Surprisingly, however, the impact of the GV mutation was strictly dependent on the presence of the proximal part of the N-terminus of CNGB1a (GARP domain) and was not observed for the short CNGB1b subunit. Unlike homomeric CNGA1 or heteromeric CNGA1/CNGB1aGV channels, channels containing CNGB1bGV displayed high sensitivity to block by L-cis-diltiazem which is the pharmacological hallmark of a functional CNGB1 subunit. The different effect of the two CNGB1 isoforms was also observed for another extensively characterised mutation impairing cGMP binding (RT>EA mutation) and was found when CNGB1a/b were assembled with another CNG A-subunit (CNCA2). Two important conclusions can be drawn from these findings. Firstly, in the absence of the GARP domain binding of cGMP to CNGB1 is not required for principal activation of heteromeric channels. This is in good agreement with a recent study showing that in the homomeric CNCA2 channel only two subunits of the tetrameric complex must bind a cyclic nucleotide to fully activate the channel [20]. Secondly, however, the presence of the GARP domain fundamentally interferes with the activation process, transforming cyclic nucleotide-binding to CNGB1 from a non-essential process to a prerequisite of channel activation. An inhibitory effect of the GARP domain on channel gating is supported by the finding that wild type rod channels have a lower open probability than rod channels lacking the GARP domain in CNGB1a. Therefore, it can be concluded that GARP is an autoinhibitory domain that controls channel activation. In the native rod CNG channel the GARP domain interacts with the channel complex (CNCA1 and CNGB1). Binding of cGMP to CNCA1 and CNGB1a relieves the inhibitory effect of GARP leading to channel opening. In channels containing a CNGB1a subunit that is deficient for cGMP binding the autoinhibitory impact of GARP cannot be removed, and CNGB1a stays locked in its closed state. This prevents the opening transition of the tetrameric channel complex even if cGMP is bound to the three CNCA1 subunits. In

the absence of the GARP domain there is no longer a constraint on channel gating. Now, binding of cGMP to the CNGA1 subunits is sufficient for full activation. The exact molecular mechanism underlying the action of the GARP domain remains to be determined. However, the co-immunoprecipitation experiments indicate that GARP can directly bind to both CNGA1 and CNGB1 suggesting that a direct protein-protein interaction underlies the effect of GARP. The GARP domain was shown to have a flexible, largely unordered structure in solution [61]. It seems possible that like other unstructured proteins such as bacterial FlgM [62] GARP can gain structure in the presence of specific binding partners. The identification of two sequences within the GARP domain that are responsible for most of its inhibitory effect supports the notion that GARP specifically interacts with the CNG channel. However, deletion of one of these regions alone was not sufficient to prevent the inhibitory effect (chapter 3.2.5). Since in this study GARP was shown to interact with both CNGB1 and CNGA1 it seems plausible that one of these regions is involved in binding to CNGB1, the second one for binding to CNGA1. Therefore, both interactions have to be disrupted to completely remove the inhibitory effect mediated by the GARP domain.

One common feature of the two inhibitory regions is the fact that they possess a unusually high percentage of negatively charged amino acids, especially glutamate. This part of the GARP domain may interfere with the N-terminus of CNGA1 that contains a positively charged lysine-rich region. The  $\alpha$ C helix of CNGB1 also harbours a high amount of positively charged residues making it a good candidate for the interaction with the GARP domain. However, the exact mechanism how the negative charge interferes with channel gating is beyond the scope of this study and remains to be determined.

In this study it could also be shown that GARP acts inhibitory if expressed as separate protein indicating that it forms an autonomous folding unit. The latter finding is important since it indicates that soluble GARP1 and GARP2 that are coexpressed together with CNGB1a in rod outer segments also can inhibit channel gating. It was proposed that the GARP domain of CNGB1a tethers the heteromeric CNG channel to the disc rim of outer segments by interacting with peripherin-2 [35, 61]. It is not known whether or not the GARP-peripherin-2 interaction competes with the interaction between GARP and the channel complex. However, even if this is the case, free soluble GARPs could still bind to the channel. This is particularly relevant for the major GARP isoform, GARP2, that contains one of the sequences conferring channel inhibition and is present in about 25 fold molar excess with respect to CNGB1a [61].

Currently, one can only speculate on physiological implications arising from the GARP-mediated inhibition of the unliganded CNG channel. Given that homomeric CNGA1 channels have a very small but detectable spontaneous open probability [63, 64] the inhibitory effect of GARP may have evolved to reduce current noise resulting from openings of CNG channels

in the absence of cGMP to the lowest possible levels. In rod outer segments only approximately 1 % of CNG channels are open in the dark and this percentage even decreases upon light-induced cGMP hydrolysis [65]. Thus, it is tempting to speculate that GARP domains to some extent contribute to the low percentage of open CNG channels and, hence, increase the sensitivity and precision of rod phototransduction. In agreement with this hypothesis, GARP domains are not present in cone photoreceptors that are much less sensitive to light.

In CNGB1a/CNGB1b KO mice [28, 29] GARP1 and GARP2 remain intact and the morphology of the rod photoreceptors is not affected by the lack of the CNGB1a subunit alone. In contrast, CNGB1 KO mice deficient for both CNGB1a and GARPs show an impaired structure of outer segments and a spoiled discs morphogenesis [36]. This supports the assumption that GARPs also function as scaffolding proteins. However, since no specific GARP1 or GARP2 KO mice are available so far, synergistic effects contributing to this phenotype cannot be excluded. Potential mutations within the GARP region in the CNGB1 locus have been identified in some patients suffering from autosomal recessive RP [36]. However, the affected families were too small to establish a causative relationship between the mutation and the disease.

Finally, this part of the study explains the clinical phenotype of patients carrying the GV mutation. Since heteromeric CNGA1/CNGB1aGV channels are inactive, rod photoreceptors of the patients cannot respond to light-induced changes in the cGMP concentration. Importantly and unlike in HEK293 cells, in rod photoreceptors CNG channel activity cannot be conferred by homomeric CNGA1 channels since these channels are not targeted to outer segments [28, 36]. Thus, the phenotype of CNGB1aGV patients is equivalent to a total knockout of the CNGB1 subunit that also results in RP [28]. However, despite the fact that GV mutation does not show any trafficking defects in HEK293 cells as shown in Fig. 15, it cannot be excluded that this mutation may cause targeting deficits *in vivo*. Therefore, to finally confirm the effects of the GV mutation on the pathogenesis of RP *in vivo*, generation of appropriate knock-in animals would be inevitable.

## 5 Summary

Rod CNG (cyclic nucleotide-gated) channels are heterotetrameric ion channels consisting of three CNGA1 and one CNGB1a subunit. To analyse the role of CNGB1a within the rod channel complex, functional consequences of two pathogenetically relevant mutations in the *CNGB1* gene were characterised. Both mutations are associated with retinitis pigmentosa (RP), a congenital progressive eye disease.

The first mutation (c.3999G>A) represents a donor site G>A transversion in exon 32 and has been proposed to result in a frameshift and truncation of the last 28 aa of the corresponding protein. However, no experimental evidence was provided for this assumption. Based on this, in a previous study it has been shown that last 28 aa of CNGB1a harbour a motif required for the proper targeting of this subunit to rod photoreceptor outer segments. This suggests defective targeting to be the major cause for the RP phenotype in affected patients. However, using exon trapping experiments, in this study it could be demonstrated that in contrast to the assumption described above the c.3999G>A mutation leads to skipping of exon 32 resulting in loss of the last 170 aa of CNGB1a. The 170 aa deletion covers the complete distal C-terminus including the last 10 aa of the important alpha  $\alpha$ C helix within the CNBD. When expressed in HEK293T cells the corresponding mutant full-length CNGB1a subunit was susceptible to proteosomal degradation. Based on these findings, apart from the defective targeting other mechanisms may be responsible for the RP phenotype in affected individuals.

The second RP associated mutation in the *CNGB1* gene (c.2978G>T; p.G993V) represents a glycine to valine exchange at the highly conserved position 993 in CNGB1a. Molecular dynamics simulations suggested that this mutation leads to major rearrangements in the cyclic nucleotide-binding domain (CNBD) that impair cGMP binding. Heteromeric CNGA1/CNGB1aGV channels were normally expressed in the plasma membrane but were functionally inactive. However, when the long N-terminal glutamic acid-rich protein (GARP) domain of CNGB1a was deleted, functional heteromeric currents were obtained in the presence of the GV mutation. Coexpression of GARP as soluble protein with the mutant heteromeric channel complex again abolished channel function. Two regions within the GARP domain that confer most of the inhibitory effect could be identified, and it could be shown that the GARP domain directly binds to the heteromeric channel complex. In conclusion, in the absence of the GARP domain binding of cGMP to CNGB1 is not required for principal activation of heteromeric CNG channels. By contrast, in the native rod photoreceptor channel, cGMP binding to CNGB1a is indispensable to relief tonic inhibition imposed by the GARP domain.

## Zusammenfassung

Zyklonukleotid-aktivierte CNG (cyclic nucleotide-gated) Kanäle aus Stäbchen sind heterotetramere Ionenkanäle bestehend aus drei CNGA1 und einer CNGB1a Untereinheit. Zur Analyse der Rolle der CNGB1a Untereinheit im Stäbchen-Kanalkomplex wurden in dieser Arbeit die funktionellen Konsequenzen von zwei pathogenetisch relevanten Mutationen im *CNGB1* Gen untersucht. Beide Mutationen sind mit Retinitis Pigmentosa (RP), einer erblichen degenerativen Augenerkrankung, assoziiert.

Bei der ersten Mutation (c.3999G>A) handelt es sich um eine G>A Transversion an der Donorstelle des Exons 32. Diese Mutation wurde ursprünglich als eine Leserasterverschiebung kategorisiert und es wurde behauptet, dass sie in einer Trunkation der letzten 28 Aminosäuren des korrespondierenden Proteins resultiert. Basierend auf dieser experimentell nicht bestätigten These wurde in einer anderen Studie gezeigt, dass die letzten 28 Aminosäuren von CNGB1a ein Motiv beherbergen, das für den Transport dieser Untereinheit in die Außensegmente der Stäbchen wichtig ist. Dies lässt vermuten, dass dem durch die c.3999G>A Mutation hervorgerufenen RP Phänotyp ein gestörter Transport von CNGB1a zu Grunde liegt. Mit Hilfe von Exon-Trapping-Experimenten konnte jedoch in dieser Arbeit nachgewiesen werden, dass im Gegensatz zur obigen Behauptung die c.3999G>A Mutation zum Überspringen von Exon 32 und infolgedessen zum Verlust der letzten 170 Aminosäuren von CNGB1a führt. Die Deletion der 170 Aminosäuren umfasst den kompletten distalen C-terminus und die letzten 10 Aminosäuren der funktionell wichtigen  $\alpha$ C-Helix innerhalb der CNBD. Die Expressionsstudie in HEK293T Zellen zeigte zudem, dass die mutierte CNGB1a Untereinheit für proteosomalen Abbau anfällig ist. Basierend auf diesen Experimenten kann geschlussfolgert werden, dass abgesehen vom gestörten Transport auch andere Mechanismen als Ursache von RP bei betroffenen Individuen in Frage kommen.

Bei der zweiten mit RP assoziierten Mutation im *CNGB1* Gen (c.2978G>T; p.G993V) handelt es sich um einen Glyzin zu Valin Austausch an der hochkonservierten Position 993 in CNGB1a. Ergebnisse der molekulardynamischen Simulation zeigten, dass diese Mutation zu einer ausgeprägten Umstrukturierung innerhalb der Bindedomäne für Zyklonukleotide (CNBD, cyclic nucleotide binding domain) führt, was mit einer Okklusion der cGMP Bindungstasche einherging. Trotz der im Vergleich zu Wildtyp-Kanälen unveränderten Plasmamembran-Expression waren die heteromeren CNGA1/CNGB1aGV Kanäle funktionell inaktiv. Nach Entfernung der langen N-terminalen glutamatreichen GARP (glutamic acid-rich protein) Domäne von CNGB1a erlangten die mutierten Kanäle jedoch ihre volle Funktion zurück. Koexpression der GARP Domäne als lösliches Protein mit dem mutierten heteromeren Kanalkomplex führte erneut zur Aufhebung der Funktion dieser Kanäle. Es wurden zwei Regionen innerhalb der GARP Domäne identifiziert, die für den größten Teil des inhibitorischen Effektes verantwortlich sind. Darüber hinaus konnte eine direkte Bindung

der GARP Domäne an den heteromeren Kanalkomplex nachgewiesen werden. Zusammenfassend lässt sich schlussfolgern, dass die cGMP Bindung an CNGB1 in Abwesenheit der GARP-Domäne für die prinzipielle Aktivierung heteromerer CNG Kanäle nicht notwendig ist. Im Gegensatz dazu stellt die Bindung von cGMP an CNGB1a im nativen Stäbchen-Kanal die Voraussetzung für die Aufhebung der tonischen Inhibition dar, welche durch die GARP Domäne vermittelt wird.

## 6 Literature

### 6.1 Cited publications

1. Hargrave, P.A. and J.H. McDowell, *Rhodopsin and phototransduction: a model system for G protein-linked receptors*. FASEB J, 1992. **6**(6): p. 2323-31.
2. Barnes, S., *After transduction: response shaping and control of transmission by ion channels of the photoreceptor inner segments*. Neuroscience, 1994. **58**(3): p. 447-59.
3. Fain, G.L., et al., *Adaptation in vertebrate photoreceptors*. Physiol Rev, 2001. **81**(1): p. 117-151.
4. Chen, C.K., et al., *Abnormal photoresponses and light-induced apoptosis in rods lacking rhodopsin kinase*. Proc Natl Acad Sci U S A, 1999. **96**(7): p. 3718-22.
5. Xu, J., et al., *Prolonged photoresponses in transgenic mouse rods lacking arrestin*. Nature, 1997. **389**(6650): p. 505-9.
6. Zhong, H., et al., *The heteromeric cyclic nucleotide-gated channel adopts a 3A:1B stoichiometry*. Nature, 2002. **420**(6912): p. 193-8.
7. Zheng, J., M.C. Trudeau, and W.N. Zagotta, *Rod cyclic nucleotide-gated channels have a stoichiometry of three CNGA1 subunits and one CNGB1 subunit*. Neuron, 2002. **36**(5): p. 891-6.
8. Weitz, D., et al., *Subunit stoichiometry of the CNG channel of rod photoreceptors*. Neuron, 2002. **36**(5): p. 881-9.
9. Peng, C., E.D. Rich, and M.D. Varnum, *Subunit configuration of heteromeric cone cyclic nucleotide-gated channels*. Neuron, 2004. **42**(3): p. 401-10.
10. Zheng, J. and W.N. Zagotta, *Stoichiometry and assembly of olfactory cyclic nucleotide-gated channels*. Neuron, 2004. **42**(3): p. 411-21.
11. Kaupp, U.B. and R. Seifert, *Cyclic nucleotide-gated ion channels*. Physiol Rev, 2002. **82**(3): p. 769-824.
12. Matulef, K. and W.N. Zagotta, *Cyclic nucleotide-gated ion channels*. Annu Rev Cell Dev Biol, 2003. **19**: p. 23-44.
13. Zagotta, W.N., et al., *Structural basis for modulation and agonist specificity of HCN pacemaker channels*. Nature, 2003. **425**(6954): p. 200-5.
14. Su, Y., et al., *Regulatory subunit of protein kinase A: structure of deletion mutant with cAMP binding domains*. Science, 1995. **269**(5225): p. 807-13.
15. Weber, I.T., et al., *Crystal structure of a cyclic AMP-independent mutant of catabolite gene activator protein*. J Biol Chem, 1987. **262**(12): p. 5630-6.
16. Trudeau, M.C. and W.N. Zagotta, *An intersubunit interaction regulates trafficking of rod cyclic nucleotide-gated channels and is disrupted in an inherited form of blindness*. Neuron, 2002. **34**(2): p. 197-207.
17. Kizhatil, K., et al., *Ankyrin-G promotes cyclic nucleotide-gated channel transport to rod photoreceptor sensory cilia*. Science, 2009. **323**(5921): p. 1614-7.
18. Altenhofen, W., et al., *Control of ligand specificity in cyclic nucleotide-gated channels from rod photoreceptors and olfactory epithelium*. Proc Natl Acad Sci U S A, 1991. **88**(21): p. 9868-72.
19. Varnum, M.D., K.D. Black, and W.N. Zagotta, *Molecular mechanism for ligand discrimination of cyclic nucleotide-gated channels*. Neuron, 1995. **15**(3): p. 619-25.
20. Biskup, C., et al., *Relating ligand binding to activation gating in CNGA2 channels*. Nature, 2007. **446**(7134): p. 440-3.
21. Waldeck, C., et al., *Activation and desensitization of the olfactory cAMP-gated transduction channel: identification of functional modules*. J Gen Physiol, 2009. **134**(5): p. 397-408.
22. Ardell, M.D., et al., *Genomic organization of the human rod photoreceptor cGMP-gated cation channel beta-subunit gene*. Gene, 2000. **245**(2): p. 311-8.

23. Colville, C.A. and R.S. Molday, *Primary structure and expression of the human beta-subunit and related proteins of the rod photoreceptor cGMP-gated channel*. J Biol Chem, 1996. **271**(51): p. 32968-74.
24. Korschen, H.G., et al., *A 240 kDa protein represents the complete beta subunit of the cyclic nucleotide-gated channel from rod photoreceptor*. Neuron, 1995. **15**(3): p. 627-36.
25. Sautter, A., et al., *An isoform of the rod photoreceptor cyclic nucleotide-gated channel beta subunit expressed in olfactory neurons*. Proc Natl Acad Sci U S A, 1998. **95**(8): p. 4696-701.
26. Chen, T.Y., et al., *A new subunit of the cyclic nucleotide-gated cation channel in retinal rods*. Nature, 1993. **362**(6422): p. 764-7.
27. Finn, J.T., M.E. Grunwald, and K.W. Yau, *Cyclic nucleotide-gated ion channels: an extended family with diverse functions*. Annu Rev Physiol, 1996. **58**: p. 395-426.
28. Huttl, S., et al., *Impaired channel targeting and retinal degeneration in mice lacking the cyclic nucleotide-gated channel subunit CNGB1*. J Neurosci, 2005. **25**(1): p. 130-8.
29. Michalakis, S., et al., *Loss of CNGB1 protein leads to olfactory dysfunction and subciliary cyclic nucleotide-gated channel trapping*. J Biol Chem, 2006. **281**(46): p. 35156-66.
30. Jenkins, P.M., et al., *PACS-1 mediates phosphorylation-dependent ciliary trafficking of the cyclic-nucleotide-gated channel in olfactory sensory neurons*. J Neurosci, 2009. **29**(34): p. 10541-51.
31. Bareil, C., et al., *Segregation of a mutation in CNGB1 encoding the beta-subunit of the rod cGMP-gated channel in a family with autosomal recessive retinitis pigmentosa*. Hum Genet, 2001. **108**(4): p. 328-34.
32. Kondo, H., et al., *A homozygosity-based search for mutations in patients with autosomal recessive retinitis pigmentosa, using microsatellite markers*. Invest Ophthalmol Vis Sci, 2004. **45**(12): p. 4433-9.
33. Korschen, H.G., et al., *Interaction of glutamic-acid-rich proteins with the cGMP signalling pathway in rod photoreceptors*. Nature, 1999. **400**(6746): p. 761-6.
34. Pentia, D.C., S. Hosier, and R.H. Cote, *The glutamic acid-rich protein-2 (GARP2) is a high affinity rod photoreceptor phosphodiesterase (PDE6)-binding protein that modulates its catalytic properties*. J Biol Chem, 2006. **281**(9): p. 5500-5.
35. Poetsch, A., L.L. Molday, and R.S. Molday, *The cGMP-gated channel and related glutamic acid-rich proteins interact with peripherin-2 at the rim region of rod photoreceptor disc membranes*. J Biol Chem, 2001. **276**(51): p. 48009-16.
36. Zhang, Y., et al., *Knockout of GARPs and the beta-subunit of the rod cGMP-gated channel disrupts disk morphogenesis and rod outer segment structural integrity*. J Cell Sci, 2009. **122**(Pt 8): p. 1192-200.
37. Shuman, S., *Novel approach to molecular cloning and polynucleotide synthesis using vaccinia DNA topoisomerase*. J Biol Chem, 1994. **269**(51): p. 32678-84.
38. Biel, M., et al., *Primary structure and functional expression of a cyclic nucleotide-gated channel from rabbit aorta*. FEBS Lett, 1993. **329**(1-2): p. 134-8.
39. Sautter, A., M. Biel, and F. Hofmann, *Molecular cloning of cyclic nucleotide-gated cation channel subunits from rat pineal gland*. Brain Res Mol Brain Res, 1997. **48**(1): p. 171-5.
40. Graham, F.L. and A.J. van der Eb, *A new technique for the assay of infectivity of human adenovirus 5 DNA*. Virology, 1973. **52**(2): p. 456-67.
41. Bradford, M.M., *A rapid and sensitive method for the quantitation of microgram quantities of protein utilizing the principle of protein-dye binding*. Anal Biochem, 1976. **72**: p. 248-54.
42. Luna, E.J., *Biotinylation of proteins in solution and on cell surfaces*. Curr Protoc Protein Sci, 2001. **Chapter 3**: p. Unit 3 6.
43. Roda, A., et al., *Nanobioanalytical luminescence: Forster-type energy transfer methods*. Anal Bioanal Chem, 2009. **393**(1): p. 109-23.

44. Griessmeier, K., et al., *Calmodulin is a functional regulator of Cav1.4 L-type Ca<sup>2+</sup> channels*. J Biol Chem, 2009. **284**(43): p. 29809-16.
45. Xia, Z. and Y. Liu, *Reliable and global measurement of fluorescence resonance energy transfer using fluorescence microscopes*. Biophys J, 2001. **81**(4): p. 2395-402.
46. Biel, M., et al., *Another member of the cyclic nucleotide-gated channel family, expressed in testis, kidney, and heart*. Proc Natl Acad Sci U S A, 1994. **91**(9): p. 3505-9.
47. Biel, M., et al., *Molecular cloning and expression of the Modulatory subunit of the cyclic nucleotide-gated cation channel*. J Biol Chem, 1996. **271**(11): p. 6349-55.
48. Pages, F., et al., *Coexpression of alpha and beta subunits of the rod cyclic GMP-gated channel restores native sensitivity to cyclic AMP: role of D604/N1201*. Biophys J, 2000. **78**(3): p. 1227-39.
49. Sunderman, E.R. and W.N. Zagotta, *Sequence of events underlying the allosteric transition of rod cyclic nucleotide-gated channels*. J Gen Physiol, 1999. **113**(5): p. 621-40.
50. Flynn, G.E., et al., *Structure and rearrangements in the carboxy-terminal region of SpIH channels*. Structure, 2007. **15**(6): p. 671-82.
51. Zhou, L. and S.A. Siegelbaum, *Gating of HCN channels by cyclic nucleotides: residue contacts that underlie ligand binding, selectivity, and efficacy*. Structure, 2007. **15**(6): p. 655-70.
52. Eswar, N., et al., *Comparative protein structure modeling using MODELLER*. Curr Protoc Protein Sci, 2007. **Chapter 2**: p. Unit 2 9.
53. Shabb, J.B. and J.D. Corbin, *Cyclic nucleotide-binding domains in proteins having diverse functions*. J Biol Chem, 1992. **267**(9): p. 5723-6.
54. Chang, Y.F., J.S. Imam, and M.F. Wilkinson, *The nonsense-mediated decay RNA surveillance pathway*. Annu Rev Biochem, 2007. **76**: p. 51-74.
55. Matulef, K. and W. Zagotta, *Multimerization of the ligand binding domains of cyclic nucleotide-gated channels*. Neuron, 2002. **36**(1): p. 93-103.
56. Mazzolini, M., M. Punta, and V. Torre, *Movement of the C-helix during the gating of cyclic nucleotide-gated channels*. Biophys J, 2002. **83**(6): p. 3283-95.
57. Biel, M. and S. Michalakis, *Cyclic nucleotide-gated channels*. Handb Exp Pharmacol, 2009(191): p. 111-36.
58. Kaupp, U.B. and R. Seifert, *Cyclic nucleotide-gated ion channels*. Physiol. Rev., 2002. **82**(3): p. 769-824.
59. Körschen, H.G., et al., *A 240 kDa protein represents the complete beta subunit of the cyclic nucleotide-gated channel from rod photoreceptor*. Neuron, 1995. **15**(3): p. 627-36.
60. Brown, R.L., et al., *Cyclic GMP contact points within the 63-kDa subunit and a 240-kDa associated protein of retinal rod cGMP-activated channels*. Biochemistry, 1995. **34**(26): p. 8365-70.
61. Batra-Safferling, R., et al., *Glutamic acid-rich proteins of rod photoreceptors are natively unfolded*. J Biol Chem, 2006. **281**(3): p. 1449-60.
62. Dedmon, M.M., et al., *FlgM gains structure in living cells*. Proc Natl Acad Sci U S A, 2002. **99**(20): p. 12681-4.
63. Ruiz, M.L. and J.W. Karpen, *Single cyclic nucleotide-gated channels locked in different ligand-bound states*. Nature, 1997. **389**(6649): p. 389-92.
64. Tibbs, G.R., E.H. Goulding, and S.A. Siegelbaum, *Allosteric activation and tuning of ligand efficacy in cyclic-nucleotide-gated channels*. Nature, 1997. **386**(6625): p. 612-5.
65. Luo, D.G., T. Xue, and K.W. Yau, *How vision begins: an odyssey*. Proc Natl Acad Sci U S A, 2008. **105**(29): p. 9855-62.

## 6.2 Own publications

### Accepted publications

**Becirovic, E.**, et al., *The retinitis pigmentosa mutation c.3444+1G>A in CNGB1 results in skipping of exon 32*. PLoS One, 2010. **5**(1): p. e8969.

Schaeferhoff K, Michalakis S, Tanimoto N, Fischer MD, **Becirovic E**, Beck SC, Huber G, Rieger N, Riess O, Wissinger B, Biel M, Seeliger MW, Bonin M  
*Induction of STAT3 related genes in fast degenerating cone photoreceptors of cpfl1 mice*  
Cellular and Molecular Life Science, 2010, May 14

**Becirovic E**, Ebermann I, Nagy D, Zrenner E, Seeliger MW, Bolz HJ. 2008. *Usher syndrome type 1 due to missense mutations on both CDH23 alleles: investigation of mRNA splicing*. Hum Mutat, 2008. **29**(3): p. 452.

Ebermann I, Scholl HP, Charbel Issa P, **Becirovic E**, Lamprecht J, et al. 2007. *A novel gene for Usher syndrome type 2: mutations in the long isoform of whirlin are associated with retinitis pigmentosa and sensorineural hearing loss*. Hum Genet, 2007. **121**(2): p. 203-11.

Michalakis S, Mühlfriedel R, Tanimoto N, Krishnamoorthy V, Koch S, Fischer MD, **Becirovic E**, Bai L, Huber G, Beck S C, Fahl E, Büning H, Paquet-Durand F, Zong X, Gollisch T, Biel M, Seeliger MW  
*Restoration of cone vision in a mouse model of congenital complete lack of cone photoreceptor function*  
Molecular Therapy, 2010 Jul 13

### Publications under review or under revision

Michalakis S\*, Zong X\*, **Becirovic E\***, Hammelmann V, Wein T, Wanner KT, Biel M  
*The role of the GARP domain in rod photoreceptor CNG channel activation*  
Submitted

\* contributed equally

Michalakis S, Kleppisch T, Wotjak C, Rammes G, Matt L, **Becirovic E**, Biel M  
*Altered synaptic plasticity and behavioral abnormalities in CNGA3-deficient mice*  
Under revision by *Genes, Brain and Behavior*

Paquet-Durand F, Beck S, Michalakis S, Goldmann T, Huber G, Mühlfriedel R, Trifunovic D, Fischer MD, Fahl E, Duetsch G, **Becirovic E**, Wolfrum U, van Veen T, Biel M, Tanimoto N, Seeliger M  
*A key role for cyclic nucleotide-gated (CNG) channels in cGMP-related retinitis pigmentosa*  
Submitted

## 7 Appendix

### 7.1 Supplementary tables and figures

1 ATGTTGGGCTGGGTCCAAAGGGTGTCTGCCTCAGCCTCCGGGGACCCCCAGAAGACTGA  
 M L G W V Q R V L P Q P P G T P Q K T E  
 21 AGAGGGAGCAGGACCACAGCCAGAAACAGAGTCAAAGCCTGAGGC AAAATCCACAACCCGA  
 E G A G P Q P E T E S K P E A N P Q P E  
 41 GCCAGAGGTTTCAGCCGGAACCCAGAGCCGGAACCCGGAACCCAGAGCCGGAACCCGGAACCCAGC  
 P E V Q P E P E P E P E P E P E P E P A  
 61 ACCTGAAGAGGCTGCACCAGAGGTCCAGACCCTGCCACCAGAGGAACCCAGTGGAAAGGAGA  
 P E E A A P E V Q T L P P E E P V E G E  
 81 GGATGTGGCTGAGGCTGGCCCTAGCCTTCAAGAGACCCAGGAAGCTGACCCTCCTCAGCC  
 D V A E A G P S L Q E T Q E A D P P Q P  
 101 CACCTCCCAGGCCCAGGTTGCTGTTGTCAAGGTGAACAGGCCCAGCTCCTGGATGTTGAG  
 T S Q A Q V A V V K V N R P S S W M L S  
 121 CTGGTTCTGGAAGGGCATGGAGAAGGTTCGTGCCACAGCCTGTCTACAGCAGCAGTGGGGG  
 W F W K G M E K V V P Q P V Y S S S G G  
 141 CCAGAACCTGGCTGCCGAGAGGGAGGCCCAGATCAGGATGGAGCACAGACCCTGGAGCC  
 Q N L A A G E G G P D Q D G A Q T L E P  
 161 CTGTGGCACTGGAGACCCAGGGTCTGAAGATGGCTCAGATAAAACTTCCAAGACTCAAGA  
 C G T G D P G S E D G S D K T S K T Q D  
 181 CACTGAGCCCAGCCTGTGGCTACTCAGGTGGCTTGAGCTGAATCTGGAGAAGGTGCTACC  
 T E P S L W L L R W L E L N L E K V L P  
 201 TCAGCCCCCTACGCCTTCCCAGGCCTGGAAAGTTGAACCTGAGGGTGCTGTCTTGGAACC  
 Q P P T P S Q A W K V E P E G A V L E P  
 221 AGATCCTCCAGGAACCCCTATGGAAGTGGAGCCCACAGAGAACCCCTCCAGCCTAATCC  
 D P P G T P M E V E P T E N P S Q P N P  
 241 TGGACCCGTGGAGCCTGAGGAGGAGCCAGCCGAGAGCCCCAGCCTGGCTTTC AAGCCTC  
 G P V E P E E E P A A E P Q P G F Q A S  
 261 TTCCCTGCCACCACCTGGGGACCTGT CAGGCTGATCGAGTGGCTCCTACACAGGCTGGA  
 S L P P P G D P V R L I E W L L H R L E  
 281 GATGGCCCTGCCTCAGCCTGTGCTCCATGGGAAGGCTGCAGAGCAGGAGCCCAGCTGCCC  
 M A L P Q P V L H G K A A E Q E P S C P  
 301 TGGGACGTGTGACGTACAGACCATCAGCATCCTCCCTGTGGAACAGGCGGAACATGATCT  
 G T C D V Q T I S I L P V E Q A E H D L  
 321 TGTCTCGAGGATGTGGACTCTTGCTGGGAGGACACCCAGCAGGAAGATGGTGGCCAGCCT  
 V L E D V D S C W E D T Q Q E D G A S L  
 341 GCAGGAGACAGAGTTGGCTCCCATTTATGAAGACGAGAGTGAGGCCATGGTGGAGATGCC  
 Q E T E L A P I Y E D E S E A M V E M P

inhibitory  
domain 1

361 CAGGGAGCTGCCA**CAGATTCAAGAGCAGCAGGAAGAGGAGAATGAAGAGAAAAGAAGA**  
 R E L P Q I Q E Q Q E E E N E E K E E E  
 381 **GGAGAAGAGAAGGAAGAGAAGGAAGAGAAGGAAGAGGAGGAAGAGAAGGAAGAGGAGGA**  
 E E E K E E K E E K E E E E E K E E E E  
 401 **GAAGAGGGAGGAAGAGAAGAAGAAAAGAGAAGGAAGAGGAGAAGAAAAGAGAAGGAAGA**  
 K R E E E K K K E K E E E K K E K E E E  
 421 **GGAGAACGGGGAGGAAGAAGAGAAGGAAGAGAAGGAAGAAAAGGAAGAGGAGGAGGGGAA**  
 E N G E E E E K E E K E E K E E E E E G K  
 441 **GGAGAAGGAAGAGAAGGAAGAGAAGGAAGAAAAGGAAGAGGAGGAGAAGGAAGAAA**  
 E E K E E K E E K E E K E E E E E K E E K  
 461 **AGAAGAGGAGGAGAAGGAAGAAAAGGAAGAGGAGGAAGAGGAAGAGGAGGAAGAGGAGGA**  
 E E E E K E E K E E E E E E E E E E E E  
 481 **AGAG**GAGCCTATTGTCCTGCTGGATAGCTGTTTGGTGGTGCAGGCTGATGTGGACCAGTG  
 E E P I V L L D S C L V V Q A D V D Q C  
 501 CCAGCTAGAAAGGGCACAGCCAGAGACAGCATCGATCCAGGAGTTACCAGAAGAAGA  
 Q L E R A Q P E T A S I Q E L P E E E E  
 521 GGAGAAGGAGGAAGAGAAGAAGGAGGAGGAAGAGGAGAAGGAGGAGGAGAAGAGAAGGA  
 E K E E E K K E E E E E K E E E E E K E  
 541 AGAGGAAGAGGAGAAGGAGGAGGAGGGGGAGGCCACAACTCAACAGTACCAGCCACGAA  
 E E E E K E E E G E A T N S T V P A T K  
 561 AGAGCACCCGGAGCTCCAGGTGGAAGACACAGATGCCGAAGCTGGCCCCCTCATCCAGA  
 E H P E L Q V E D T D A E A G P L I P E  
 581 GGAGACGATCCCGCCACCTGAGAGACCACAGTGTCTCCCGCCAAGTCTGACACCCTCGC  
 E T I P P P E R P P V S P A K S D T L A  
 601 GGTTCACGCGCAGCAACCCACAGGAAGAAGCTACCTTCTCAGGATGATGAGGCTGAAGA  
 V P S A A T H R K K L P S Q D D E A E E  
 621 ACTCAAGGCCCTGTACCCGGCTGAGTCCCCAGTGGTTGCCTGGTCAGACCCCACCACCCC  
 L K A L S P A E S P V V A W S D P T T P  
 641 ACAGGAGGCTGATGGCGAGGACCGTGC GGCCCTCCACAGCCAGCCAGAACAGTGCCATCAT  
 Q E A D G E D R A A S T A S Q N S A I I  
 661 CAACGACCCGGCTCCAGGAGCTGGTGAAGATGTTCAAGGAGCGGACAGAGAAGGTGAAGGA  
 N D R L Q E L V K M F K E R T E K V K E  
 681 GAAGCTCATTGACCCTGACGTCACCTCCGATGAGGAGAGCCCCAAGCCCTCCCAGCCAA  
 K L I D P D V T S D E E S P K P S P A K  
 701 GAAGCCCCAGACTCAGCCCCAGCCAGAAGCCGGCGGAGGCAGAGCGGCAGAGGAGGA  
 K A P D S A P A Q K P A E A E A A E E E  
 721 GCACTACTGTGACATGCTCTGCTGCAAATTTAAGCGCAGGCCCTGGAAGATGTACCAGTT  
 H Y C D M L C C K F K R R P W K M Y Q F  
 741 CCCCCAGGCATCGACCCACTGACCAACCTC**S1**ATGTACATCCTGTGGCTGTTCTTCGTGGT  
 P Q S I D P L T N L M Y I L W L F F V V  
 761 **GCTGGCCTGGA**ACTGGA**S1**CTGGCTGATTCTGTGCGCTGGGCCCTTCCCGTACCAGCG  
 L A W N W N C W L I P V R W A F P Y Q R

inhibitory  
domain 2

781 GGCAGACAACATCCACCTCTGGCTGCTCATGGACTACTTGTGCGACTTCATCTACCTCCT  
A D N I H L W L L M D Y L C D F I Y L L

801 **GGACATCACCGTG**TTCCAGATGCGTCTCCAGTTTGTCAAAGGCGGGGACATCATTACAGA  
D I T V F Q M R L Q F V K G G D I I T D

821 TAAGAAGGAGATGCGTAATAATTACCTGAAGTCTCAACGATTTAAGATGGACTTGCTCTG  
K K E M R N N Y L K S Q R F K M D L L C

841 **CCTTTTGCCTTTGGATTTTCTCTACTTTGAAACTTGGCGTGAACCCCTTCTTCGCCTGCC**  
L L P L D F L Y L K L G V N P L L R L P

861 **CCGCTGCCTGAAGTACATGGCCTTCTTTGAGTTTAATAACCGTCTGGAAGCCATCCTCAG**  
R C L K Y M A F F E F N N R L E A I L S

881 CAAAGCCTACGTTTACAGGGTATCAGGACCACCGCCTACCTGCTGTATAGCTTGCATCT  
K A Y V Y R V I R T T A Y L L Y S L H L

901 **CAACTCCTGTCTTTACTACTGGGCGTCGGCCTTCCAGGGCATCGGTTCCACTCACTGGGT**  
N S C L Y Y W A S A F Q G I G S T H W V

921 TTATGACGGCGTGGGGAACAGCTACATTCGATGCTACTACTGGGCTGTGAAACTCTCAT  
Y D G V G N S Y I R C Y Y W A V K T L I

941 CACCATCGGAGGACTGCCCGACCCAGACGCTCTTTGAGATCGTCTTCCAGCTGCTGAA  
T I G G L P D P Q T L F E I V F Q L L N

961 **TTATTTTACAGGTGTCTTTCGCTTTCTCTGTGATGATTGGA**CAGATGAGAGATGTGGTGGG  
Y F T G V F A F S V M I G Q M R D V V G

981 GGCCGCCACGGCAGGGCAGACGTACTACCGCAGCTGCATGGACAGCACGGTGAAGTACAT  
A A T A G Q T Y Y R S C M D S T V K Y M

1001 GAACTTCTACAAGATCCCCAGGTCTGTGCAGAACCGCGTCAAGACCTGGTACGAATACAC  
N F Y K I P R S V Q N R V K T W Y E Y T

1021 CTGGCACTCACAAGGCATGCTGGATGAGTCAGAGCTGATGGTTCAGCTTCCGGACAAGAT  
W H S Q G M L D E S E L M V Q L P D K M

1041 GCGTCTGGACCTGGCCATTGACGTAAACTACAACATTGTCAGCAAAGTGGCGCTCTTCCA  
R L D L A I D V N Y N I V S K V A L F Q

1061 GGGCTGCGACCGGCAGATGATCTTCGACATGCTCAAGCGACTTCGCTCAGTCGTCTACCT  
G C D R Q M I F D M L K R L R S V V Y L

1081 **ACCCAATGACTATGTGTGCAAGAAGGGGGAGATTGGCCGAGAGATGTATATTATCCAGGC**  
P N D Y V C K K G E I G R E M Y I I Q A

1101 **GGGGCAGGTGCAGGTGCTGGGCGGCCAGATGGAAAGGCTGCTCTGGTGACACTCAAAGC**  
G Q V Q V L G G P D G K A V L V T L K A

1121 **CGGATCGGTGTTTTGGAGAGATAAGCTTGCTGGCTGTCTGGGGCGGTAACAGGCGCACGGC**  
G S V F G E I S L L A V G G G N R R T A

1141 **CAATGTGGTGGCCACGGCTTACCAATCTCTTCACTTCTGGATAAGAAGGACTTGAATGA**  
N V V A H G F T N L F I L D K K D L N E

1161 **GATTTTGGTGCATTACCTGAATCTCAGAAGCTGCTCCGGAAGAAGGCCAGGCGCATGCT**  
I L V H Y P E S Q K L L R K K A R R M L

1181 **CAGAAACAACAACAACCAAGGAGGAGAAG**AGTGTGCTCATCTGCCCCACGTGCGGG  
R N N N K P K E E K S V L I L P P R A G

```

1201  CACCCCGAAGCTCTTCAATGCTGCCCTGGCTGCAGCAGGAAAGATGGGCCCCAGGGGAGC
      T P K L F N A A L A A A G K M G P R G A

1221  CAAGGGCGGCAAGCTCGCCACCTGAGAGCCAGGCTCAAAGAAGCTGGCTGCACTGGAGGC
      K G G K L A H L R A R L K E L A A L E A

1241  AGCCGCACGACAGCAGCAGCTGCTGGAACAGGCCAAGAGCTCGCAAGAAGCCGGGGGAGA
      A A R Q Q Q L L E Q A K S S Q E A G G E

1261  GGAGGGCTCTGGAGCCACAGACCAACCTGCACCCAGGAGCCGTCAGAGCCCAAGGAGCC
      E G S G A T D Q P A P Q E P S E P K E P

1281  CCCGGAGCCCCCAGCCCCGAGTTCTCCACCGCCAGCCTCAGCAAAGCCCGAGGGAAGCAC
      P E P P A P S S P P P A S A K P E G S T

1301  GGAGGAGGCCGCGAGGGCCCGGAGCCTTCAGTGAGGATCCGTGTGAGTCCAGGCCCTGA
      E E A A G P P E P S V R I R V S P G P D

1321  TCCCGGGGAACAGACACTATCGGTGGAGATGCTGGAAGAGAAGAAGGAGGAGGTGGAG
      P G E Q T L S V E M L E E K K E E V E

```

**Suppl. Fig. 1 Structural features of the rat CNGB1a.** Shown are the two regions within the GARP domain which confer the most part of the inhibitory effect as measured by L-cis-diltiazem sensitivity (cf. Fig. 17). For better orientation, six transmembrane domains (S1-S6) and cyclic nucleotide binding domain (CNBD, blue font) are also highlighted within the sequence. Numbers on the left refer to the amino acid positions at the beginning of each line.

**Suppl. Table 1 List of primer used for the synthesis of different mutagenesis constructs.** 1+2: mutagenesis for CNGB1aGV, 3+4 B1a#556-1339, 5+6  $\Delta$ 214-555, 5+7 B1a#1-555, 8+10  $\Delta$ 1-481, 9+10  $\Delta$ 1-363.

	Name	Gene	Sequence 5'-3'
1	B1_MutG-V_F	Rat CNGB1	ATGTGTGCAAGAAGGTGGAGATTGGCCGAG
2	B1_MutG-V_R	Rat CNGB1	CTCGGCCAATCTCCACCTTCTTGACACAT
3	Oligo HindXho1	Rat CNGB1	AGCTTGAATTCGCCACCATGGTAC
4	Oligo HindXho2	Rat CNGB1	CATGGTGGCGAATTCA
5	B1aKpnfor	Rat CNGB1	CTATAGGGAGACCCAAGCTTGG
6	KpnAAErev	Rat CNGB1	CCGGTACCTCTGCGGCTGGCTCCTCC
7	B1aTNSTXbarev	Rat CNGB1	CCTCTAGAGCTGTTGAGTTTGTGTCCT
8	KpnKzkEPIV_F	Rat CNGB1	CCGGTACCGCCACCATGGAGCCTATTGTCCTGCTGG
9	KpnKzkPQIQfor	Rat CNGB1	CCGGTACCGCCACCATGCCACAGATTCAAGAGCAGC
10	B1BsrGrev	Rat CNGB1	CGAAGAACAGCCACAGGATG

**Suppl. Table 2 List of primer used for amplification of different human CNG channel constructs.**

	Name	Gene	Sequence 5'-3'
1	hB1aKzkBamfor	Human CNGB1	CCGGATCCACCGCCATGTTGGGCTGGGTCCAGAG
2	hB1Xhorev	Human CNGB1	GGCTCGAGTCCGCCTTCTCCTCCCTTTC
3	KpnKzkhB1adNTfor	Human CNGB1	CCGGTACCGCCACCATGGTGCCTGCCACGAAACAGC
4	hA1KzkEcofor	Human CNGA1	CCGAATTCACCGCCATGAAACTATCCATGAAGAAC
5	hA1Salrev	Human CNGA1	CCGTCGACTATGTAGAGTCGATGGGCC
6	hB1G993Vfor	Human CNGB1	ACTATGTGTGCAAGAAGGTGGAGATCGGCCGTGAGAT
7	hB1G993Vrev	Human CNGB1	ATCTCACGGCCGATCTCCACCTTCTTGCACACATAGT
8	KzkhNT9for	Human CNGB1	GCCACCATGTCCCGGATTGAAGAGGAGAAAAG
9	KzkhNT8for	Human CNGB1	GCCACCATGGTGACTGAGGTGCTGCTGG

**Suppl. Table 3 List of primer used for the synthesis of FRET constructs. 1+2, YFP-CNGB1a. 3+4 CNGA1-CFP.**

	Name	Gene	Sequence 5'-3'
1	YFPKpnfor	Rat CNGB1	GTCGGTACCATGGTGAGCAAGGGCG
2	YFPB1rev	Rat CNGB1	GACCCAGCCCAACATCTTGTACAGCTCGTCCATGCC
3	InfmA1CFPfor	Bovine CNGA1	GGGAAAGTGGGCCACAGACTCTACACAGGAC
4	InfmA1CFPrev	Bovine CNGA1	CTATAGAATAGGGCCCTCTAGATGCATGC

**Suppl. Table 4 Primer used for PCR amplification of minigene constructs and splice products (1-4). Numbers 5-6 represent the primer used for site directed mutagenesis (introduction of the c.3444+1G>A mutation).**

	Name	Gene/Vector	Sequence 5'-3'
1	hB1a_in30F	Human CNGB1	CGAAACGGCAGTCTCTGAAGG
2	hB1a_e33R	Human CNGB1	CACACCTGCTGGAAGTGC
3	pcDNA3_F	pcDNA3	CTAGAGAACCCACTGCTT
4	pcDNA3_R	pcDNA3	GCACAGTCGAGGCTGATC
5	hB1aKondoF	Human CNGB1	GAGTTGGTGGAACAGATAATGTGGTTGGGAAC
6	hB1aKondoR	Human CNGB1	GTTCCAACACATTATCTGTTCCACCAACTC

**Suppl. Table 5 Antibodies used in this study.**

<b>Antibody</b>	<b>Source</b>	<b>Dilution</b>	<b>Secondary antibody</b>	<b>Dilution</b>
anti-ATPase clone $\alpha$ 6F	Developed by D.M. Fambrough, obtained from the Developmental Studies Hybridoma Bank	1:1000	anti-mouse	1:2000
anti-CNGB1	Hüttl 2005 J Neurosci	1:10000	anti-rabbit	1:2000
anti-GFP	Clontech, Mountain View	1:1000	anti-mouse	1:2000
anti-myc clone 9B11	New England Biolabs	1:1000	anti-mouse	1:2000
PPc6N	Colville CA, Molday RS [23]	1:1000	anti-rabbit	1:2000
anti-tubulin	Dianova, Hamburg, Germany	1:400	anti-mouse	1:2000

## 7.2 Abbreviations

aa	amino acids
BES	N-N-Bis(2-hydroxyethyl)-2-aminoethanesulfonic acid
bp	base pairs
BSA	bovine serum albumin
cAMP	cyclic adenosine monophosphate
CAP	catabolite gene activator protein
cDNA	complementary DNA
CFP	cyan fluorescent protein
cGMP	cyclic guanosine monophosphate
CMV	cytomegalovirus
CNBD	cyclic nucleotide-binding domain
CNG	cyclic nucleotide-gated
ddH <sub>2</sub> O	double deionized water
DEPC	diethyl pyrocarbonate
DMEM	Dulbecco's modified eagle medium
DMSO	dimethylsulfoxide
DNA	deoxyribonucleic acid
dNTP	2'-desoxynucleoside-5'-triphosphate (dATP, dCTP, dGTP, dUTP or dTTP)
DTT	dithiothreitol
<i>E. coli</i>	Escherichia coli
EDTA	ethylenediaminetetraacetic acid
GFP	green fluorescent protein
FBS	fetal bovine serum
h	hour
HCl	hydrochloric acid
HCN	hyperpolarisation activated cyclic nucleotide-gated channel
HEK293	human embryonic kidney cells
HRP	horseradish peroxidase
IgG	immunoglobulin G
kb	kilobase pairs
kDa	kilodalton
KO	knockout
LB broth	Luria-Bertani broth
mA	milliampere
MD	molecular dynamics
MCS	multiple cloning site
mg	milligram
min	minute
mL	milliliter
MOPS	3-[N-Morpholino]propanesulfonic acid
mRNA	messenger RNA
μg	microgram
NMD	nonsense mediated mRNA decay
NP-40	nonyl phenoxy polyethoxy ethanol
Ori	origin of replication

---

PBS	phosphate buffered saline
PCR	polymerase chain reaction
PFA	Paraformaldehyde
PKA	cAMP dependent protein kinase
$P_{\max}$	maximal channel open probability
pmol	picomol
PVP	polyvinylpyrrolidone
RNA	ribonucleic acid
RNase	ribonulease
RP	retinitis pigmentosa
Rpm	rotations per minute
RT-PCR	reverse transcriptase PCR
SDS	sodium dodecylsulfate
sec	second
TEMED	N,N,N',N'-Tetramethylethylenediamine
TRIS	tris(hydroxymethyl)aminomethane
UV	ultraviolet
WT	wild type
YFP	yellow fluorescent protein

### 7.3 Curriculum Vitae

#### Personal Information

Name: Elvir Becirovic  
Place of birth: Sarajevo, Bosnia and Hercegovina  
Date of birth: 04.05.1979  
Nationality: Bosnian  
Adress: Fürstenrieder Str. 282 81377 München  
Email: elvir.becirovic@cup.uni-muenchen.de  
Marital status: unmarried

#### Education

2007-present PhD at the Department of Pharmacy - Center for Drug Research, Ludwig-Maximilians-Universität München, Germany

2001-2006 Study of biology at the University of Cologne, Germany  
Degree: Diploma in biology (Dipl. Biol)

1994-2000 Comprehensive school (Europaschule Köln-Zollstock) in Cologne, Germany  
Degree: general qualification for university entrance (allgemeine Hochschulreife)

1992-1993 Exterritorial primary school in Nagyatad, Hungary

1986-1992 Primary school in Modrica, Bosnia and Hercegovina

#### Publications

**Becirovic, E.**, et al., *The retinitis pigmentosa mutation c.3444+1G>A in CNGB1 results in skipping of exon 32*. PLoS One, 2010. **5**(1): p. e8969.

Schaeferhoff K, Michalakis S, Tanimoto N, Fischer M D, **Becirovic E**, Beck SC, Huber G, Rieger N, Riess O, Wissinger B, Biel M, Seeliger MW, Bonin M  
*Induction of STAT3 related genes in fast degenerating cone photoreceptors of cpfl1 mice*  
Cellular and Molecular Life Science, 2010, May 14

**Becirovic E**, Ebermann I, Nagy D, Zrenner E, Seeliger MW, Bolz HJ. 2008. *Usher syndrome type 1 due to missense mutations on both CDH23 alleles: investigation of mRNA splicing*. Hum Mutat, 2008. **29**(3): p. 452.

Ebermann I, Scholl HP, Charbel Issa P, **Becirovic E**, Lamprecht J, et al. 2007. *A novel gene for Usher syndrome type 2: mutations in the long isoform of whirlin are associated with retinitis pigmentosa and sensorineural hearing loss*. Hum Genet, 2007. **121**(2): p. 203-11.

Michalakis S, Mühlfriedel R, Tanimoto N, Krishnamoorthy V, Koch S, Fischer MD, **Becirovic E**, Bai L, Huber G, Beck S C, Fahl E, Büning H, Paquet-Durand F, Zong X, Gollisch T, Biel M, Seeliger MW  
*Restoration of cone vision in a mouse model of congenital complete lack of cone photoreceptor function*  
Molecular Therapy, 2010 Jul 13

### Conferences and Presentations

- |              |  |
|--------------|--|
| March 2010   | 51th Annual Meeting of the DGPT (Deutsche Gesellschaft für Experimentelle und Klinische Pharmakologie und Toxikologie) in Mainz, Germany:<br>oral presentation |
| October 2009 | European Retina Meeting 2009 in Oldenburg (Oldenburg), Germany:<br>poster presentation   |
| June 2009    | 4 <sup>th</sup> International Conference on cGMP in Regensburg (Germany)   |

## Lebenslauf

### Persönliche Angaben

Name: Elvir Becirovic  
Geburtsort: Sarajevo, Bosnien und Herzegowina  
Geburtsdatum: 04.05.1979  
Nationalität: Bosnisch  
Adresse: Fürstenrieder Str. 282 81377 München  
Email: elvir.becirovic@cup.uni-muenchen.de  
Familienstand: ledig

### Ausbildung

1986-1992                      Grundschule in Modrica, Bosnien und Herzegowina  
1992-1993                      Exterritoriale Grundschule in Nagyatad, Ungarn  
1994-2000                      Europaschule Köln, Gesamtschule Zollstock  
Abschluss: Allgemeine Hochschulreife  
2001-2006                      Biologiestudium an der Universität zu Köln  
Abschluss: Diplom  
2007-heute                      PhD am Department für Pharmazie - Center for Drug Research,  
Ludwig-Maximilians-Universität München

### Publikationen

**Becirovic, E.**, et al., *The retinitis pigmentosa mutation c.3444+1G>A in CNGB1 results in skipping of exon 32*. PLoS One, 2010. **5**(1): p. e8969.

Schaeferhoff K, Michalakis S, Tanimoto N, Fischer MD, **Becirovic E**, Beck SC, Huber G, Rieger N, Riess O, Wissinger B, Biel M, Seeliger MW, Bonin M  
*Induction of STAT3 related genes in fast degenerating cone photoreceptors of cpfl1 mice*  
Cellular and Molecular Life Science, 2010, May 14.

**Becirovic E**, Ebermann I, Nagy D, Zrenner E, Seeliger MW, Bolz HJ. 2008. *Usher syndrome type 1 due to missense mutations on both CDH23 alleles: investigation of mRNA splicing*. Hum Mutat, 2008. **29**(3): p. 452.

Ebermann I, Scholl HP, Charbel Issa P, **Becirovic E**, Lamprecht J, et al. 2007. *A novel gene for Usher syndrome type 2: mutations in the long isoform of whirlin are associated with retinitis pigmentosa and sensorineural hearing loss*. Hum Genet, 2007. **121**(2): p. 203-11.

Michalakis S, Mühlfriedel R, Tanimoto N, Krishnamoorthy V, Koch S, Fischer MD, **Becirovic E**, Bai L, Huber G, Beck S C, Fahl E, Büning H, Paquet-Durand F, Zong X, Gollisch T, Biel M, Seeliger MW  
*Restoration of cone vision in a mouse model of congenital complete lack of cone photoreceptor function*  
Molecular Therapy, 2010 Jul 13

### Konferenzen und Präsentationen

- |              |   |
|--------------|---|
| März 2010    | 51th Annual Meeting of the DGPT (Deutsche Gesellschaft für Experimentelle und Klinische Pharmakologie und Toxikologie) in Mainz:<br>Vortrag |
| Oktober 2009 | European Retina Meeting 2009 in Oldenburg (Oldenburg):<br>Poster Präsentation   |
| Juni 2009    | 4 <sup>th</sup> International Conference on cGMP in Regensburg  |

#### 7.4 Acknowledgements/Danksagung

Mein größter Dank gilt meiner Familie - ohne ihre Unterstützung wäre diese Arbeit wie auch meine bisherige wissenschaftliche Karriere kaum möglich gewesen. Deswegen widme ich diese Arbeit meiner Familie und hoffe, dass ich hiermit einen kleinen Teil zurückgeben kann.

Besonders danken möchte ich auch meinem Betreuer Stelios, der mir auch in schwierigen Zeiten immer zur Hilfe stand und meinen wissenschaftlichen Ehrgeiz (nicht selten gegen meinen Willen) immer vorangetrieben hat. Steffi, Susanne, Verena, Stelios und Prof. Biel danke ich auch für das Korrekturlesen dieser Arbeit. Bei Prof. Biel möchte ich mich außerdem für seine wissenschaftlichen Ratschläge herzlich bedanken sowie für die Möglichkeit, diese Arbeit in seinem Arbeitskreis durchführen zu können.

Dr. Xiangang Zong danke ich für die nette und gute Zusammenarbeit und dafür, dass er mir seine Messdaten zur Verfügung gestellt hat. Ebenfalls danken möchte ich Prof. Wanner und Thomas Wein für die Ergebnisse der molekulardynamischen Simulation, die in dieser Arbeit gezeigt wurden.

Eine ganz entscheidende Rolle für das Gelingen dieser Arbeit haben meine jetzigen und ehemaligen Arbeitskollegen gespielt. Die lustige Arbeitsatmosphäre und die vielen (teilweise noch viel lustigeren) privaten Unternehmungen haben mein Durchhaltevermögen gestärkt und so manch eine frustrierte Stunde viel erträglicher gemacht. Nicht zuletzt, weil sie mit meiner ironischen und sehr launenhaften Umgangsart immer umzugehen wussten, möchte ich mich deshalb an dieser Stelle (diesmal vollkommen ironiefrei) bei ihnen vom ganzen Herzen bedanken und wünsche allen beruflich und privat alles Gute.